JNeurosci
THE JOURNAL OF NEUROSCIENCE

Research Articles: Cellular/Molecular

miR126-5p down-regulation facilitates axon degeneration and NMJ disruption via a non-cell-autonomous mechanism in ALS

Roy Maimon[1], Ariel Ionescu[1], Avichai Bonnie[1], Sahar Sweetat[2], Shane Wald-Altman[3], Shani Inbar[3], Tal Gradus[1], Davide Trotti[4], Miguel Weil[3], Oded Behar[2] and Eran Perlson[1]

[1]*Department of Physiology and Pharmacology, Sackler Faculty of Medicine, Tel Aviv University, Tel Aviv 69978, Israel*

[2]*Department of Developmental Biology and Cancer Research, The Hebrew University of Jerusalem, Israel*

[3]*Department of Cell Research and Immunology, Tel Aviv University, Israel*

[4]*Jefferson Weinberg ALS Center, Vickie and Jack Farber Institute for Neuroscience, Department of Neuroscience, Thomas Jefferson University, Philadelphia, USA*

DOI: 10.1523/JNEUROSCI.3037-17.2018

Received: 22 October 2017

Revised: 15 April 2018

Accepted: 23 April 2018

Published: 17 May 2018

Author contributions: R.M., A.I., M.W., O.B., and E.P. designed research; R.M., A.I., A.B., S.S., S.I., S.W.-A., and T.G. performed research; S.W.-A., D.T., and M.W. contributed unpublished reagents/analytic tools; R.M., A.I., A.B., S.S., S.I., T.G., O.B., and E.P. analyzed data; R.M., A.I., M.W., O.B., and E.P. wrote the paper.

Conflict of Interest: The authors declare no competing financial interests.

This work was supported by the Rosetrees trust, Alfred Taubman, the IsrALS Foundation, the Israel Science Foundation (grant number 561-11), and the European Research Council (grant number 309377) to E.P. The Israel Science Foundation, grant number 947/14 to O.B. and The National Institutes of Health (NIH) grant (RO1-NS44292) to D.T. We thank Dr. Eran Horenstein for miR126 and miR 142, as well as for extra SOD1G93A mice. We also thank Dr. Mickey Harlev and Lior Bikovski for assisting with mouse injection and the behavioral tests. Lastly, we thank Konstantin Voloshin, for his help in NMJ analysis.

Correspondence should be addressed to corresponding author: Eran Perlson, Ph.D., Dept. of Physiology and Pharmacology, Sackler Faculty of Medicine, Room 605, Sagol School of Neuroscience, Tel Aviv University, Ramat Aviv, Tel Aviv 69978, Israel. +972-3-6408743, E-mail: eranpe@post.tau.ac.il; Oded Behar, Ph.D., Dept. of Developmental Biology and Cancer Research, The Institute for Medical Research, Faculty of Medicine, The Hebrew University, Ein Kerem, P.O. Box 12271, Jerusalem, 91120 Israel. +972-2-6758470, E-mail: odedb@ekmd.huji.ac.il

Cite as: J. Neurosci ; 10.1523/JNEUROSCI.3037-17.2018

Title: miR126-5p down-regulation facilitates axon degeneration and NMJ disruption via a non-cell-autonomous mechanism in ALS

Abbreviated title – miR126-5p dysregulation in ALS physiology

Authors: Roy Maimon[1*], Ariel Ionescu[1*], Avichai Bonnie[1], Sahar Sweetat[2], Shane Wald-Altman[3], Shani Inbar[3], Tal Gradus[1], Davide Trotti[4], Miguel Weil[3], Oded Behar[2#], and Eran Perlson[1#]

[1]Department of Physiology and Pharmacology, Sackler Faculty of Medicine, Tel Aviv University, Tel Aviv 69978, Israel
[2]Department of Developmental Biology and Cancer Research, The Hebrew University of Jerusalem, Israel
[3]Department of Cell Research and Immunology, Tel Aviv University, Israel
[4]Jefferson Weinberg ALS Center, Vickie and Jack Farber Institute for Neuroscience, Department of Neuroscience, Thomas Jefferson University, Philadelphia, USA

* The first two authors contributed equally to this work.

[#]**corresponding author**:

Eran Perlson, Ph.D., Dept. of Physiology and Pharmacology, Sackler Faculty of Medicine, Room 605, Sagol School of Neuroscience, Tel Aviv University, Ramat Aviv, Tel Aviv 69978, Israel. +972-3-6408743
E-mail: eranpe@post.tau.ac.il

Oded Behar, Ph.D., Dept. of Developmental Biology and Cancer Research
The Institute for Medical Research, Faculty of Medicine, The Hebrew University, Ein Kerem, P.O. Box 12271, Jerusalem, 91120 Israel. +972-2-6758470
E-mail: odedb@ekmd.huji.ac.il

Number of pages – 39 **Number of figures** – 6 + 11 extended data figures
Number of movies – 6
Number of words for: Abstract – 136; Introduction – 1247; Discussion - 1648

Conflict of interest: The authors declare no competing financial interests

Acknowledgments: This work was supported by the Rosetrees trust, Alfred Taubman, the IsrALS Foundation, the Israel Science Foundation (grant number 561-11), and the European Research Council (grant number 309377) to E.P. The Israel Science Foundation, grant number 947/14 to O.B. and The National Institutes of Health (NIH) grant (RO1-NS44292) to D.T. We thank Dr. Eran Horenstein for miR126 and miR 142, as well as for extra SOD1^{G93A} mice. We also thank Dr. Mickey Harlev and Lior Bikovski for assisting with mouse injection and the behavioral tests. Lastly, we thank Konstantin Voloshin, for his help in NMJ analysis.

Abstract

Axon degeneration and disruption of neuromuscular junctions (NMJs) are key events in Amyotrophic Lateral Sclerosis (ALS) pathology. Although the disease's etiology is not fully understood, it is thought to involve a non-cell-autonomous mechanism and alterations in RNA metabolism. Here, we identified reduced levels of miR-126-5p in pre-symptomatic ALS male mice models, and an increase in its targets: axon destabilizing type-3 Semaphorins and their co-receptor Neuropilins. Utilizing compartmentalized *in vitro* co-cultures, we demonstrated that myocytes expressing diverse ALS-causing mutations promote axon degeneration and NMJ dysfunction, which were inhibited by applying Neuropilin1 (NRP1) blocking antibody. Finally, overexpressing miR126-5p is sufficient to transiently rescue axon degeneration and NMJ disruption both *in vitro* and *in vivo*. Thus, we demonstrate a novel mechanism underlying ALS pathology, in which alterations in miR126-5p facilitate a non-cell-autonomous mechanism of motor neuron degeneration in ALS.

Significance Statement

In spite of some progress, currently no effective treatment is available for ALS. We suggest a novel regulatory role for miR126-5p in ALS and demonstrate for the first time a mechanism by which alterations in miR126-5p contribute to axon degeneration and NMJ disruption observed in ALS. We show that miR126-5p is altered in ALS models and that it can modulate Sema3 and NRP protein expression. Furthermore, NRP1 elevations in motor neurons and muscle secretion of Sema3A contribute to axon degeneration and NMJ disruption in ALS. Finally, overexpressing miR126-5p is sufficient to transiently rescue NMJ disruption and axon degeneration both *in vitro* and *in vivo.*

Introduction

Amyotrophic lateral sclerosis (ALS) is a lethal neurodegenerative disease that affects motor neurons (MNs) in the cortex, brain stem, and spinal cord (Mulder et al., 1986; Peters et al., 2015). It is characterized by neuromuscular junction (NMJ) disruption, MN axon degeneration, and neuronal death (Frey et al., 2000; Fischer et al., 2004; Moloney et al., 2014). In spite of some progress, currently no effective treatment is available for ALS. The diversity of ALS-related mutations has given rise to the use of numerous animal models with diverse phenotypes, ranging from no effect on motor neuron function to severe progressive paralysis (Philips and Rothstein, 2015). About 20% of familial ALS (fALS) is accounted for by mutations in the superoxide dismutase 1 (SOD1) gene (Scrutton et al., 1992; Rosen et al., 1993; Gurney et al., 1994). Mutations in the SOD1 gene (mSOD1) have also been described in sporadic cases (sALS) (Rakhit et al., 2004). Other mutations found in ALS patients include hexanucleotide expansion repeats in the *C9orf72* locus, which lead to various di-peptide repeats, e.g., Proline-Arginine or Glycine-Arginine repeats (PR_{50} and GR_{50}, respectively), and in the gene encoding the TDP43 RNA binding protein (Buratti, 2015; Wen et al., 2016). An efficient method for studying NMJ stability and health *in vitro* is by using the microfluidic chamber (MFC) system, which allows the culture of primary myocytes in one compartment, and motor neurons in the other, thus setting up conditions conducive to generating active NMJs (Zahavi et al., 2015).

The neurodegeneration that occurs in ALS is considered to be a non-cell autonomous process involving interactions between the neuron and its diverse extracellular microenvironments via an unknown mechanism (Ilieva et al., 2009; Tsitkanou et al., 2016). Although the molecular basis for neuronal dysfunction and death in ALS is still poorly understood, it may be due to alterations in the nature of the extracellular signaling pathways that switch from pro-survival to toxic (Ilieva et al., 2009; Perlson et al., 2009). Numerous studies support the notion that multiple tissues outside the CNS, including skeletal muscle (Dupuis et al., 2006; Tsitkanou et al., 2016), astrocytes (Nagai et al., 2007), and microglia (Lee et al., 2016) contribue to ALS pathologies. Alterations in RNA metabolism and microRNAs (miRs) can contribute to, and also be part of mechanisms that initiate the disease (Lemmens et al., 2010; Emde and Hornstein, 2014). miRs are post-transcriptional regulators that play an important role in many cellular processes like axon growth and retraction, and were demonstrated to be involved in many diseases including neurodegenerative diseases such as ALS (Hawley et al., 2017; Molasy et al., 2017).

Alterations in miR expression profile were identified specifically in axons of ALS models (Rotem et al., 2017), as well in muscles leading to increasing attempts to either use or target miRs as therapeutic strategies (Di Pietro et al., 2017). Therefore, it is reasonable to assume that alterations in RNA and miRNA metabolism, of both MNs and neighboring cells, can regulate a secreted destabilizing signal, which in turn, facilitates axon degeneration and NMJ disruption.

Semaphorin3A (Sema3A) was initially identified as a repellent guidance molecule (Luo et al., 1993; Worzfeld and Offermanns, 2014). However, later works showed that it can also induce neuronal cell death of sympathetic, sensory, retinal, and cortical neurons (Nakamura et al., 2000; Shirvan et al., 2002; Ben-Zvi et al., 2008; Jiang et al., 2010). Neuropilin1 (NRP1) has been shown to be the receptor binding component for Sema3A as well as some other type 3 Semaphorins (Kolodkin et al., 1997). Sema3A was found to be up-regulated following central nervous system injury as well as in several neurodegenerative diseases (Kaneko et al., 2006; Van Battum et al., 2015). Importantly, Sema3A was found to be up-regulated in terminal Schwann cells (TSCs) of the $SOD1^{G93A}$ transgenic mouse model for ALS and in the motor cortex of ALS patients (De Winter et al., 2006; Körner et al., 2016), suggesting that it plays a toxic role in disease pathology and progression.

Here we demonstrated that alterations in miR126-5p result in up-regulation of type 3 Semaphorins and its co-binding receptor NRP1 in muscles and MN axons of ALS models, respectively. We further demonstrate *in vitro* and *in vivo* the contribution of this pathway to axon degeneration and NMJ disruption in ALS models.

Materials and Methods

Animals and vector injections

HB9::GFP (Stock No: 005029) mice were originally obtained from Jackson Laboratories. The colony was maintained by breeding with ICR mice.
$SOD1^{G93A}$ (Stock No: 002726) mice were originally obtained from Jackson Laboratories, and maintained by breeding with C57BL/6J mice. Genotyping was performed using the polymerase chain reaction (KAPA Bio systems); DNA samples were generated from ear or tail tissue biopsies.
All injection procedures were performed on pre-symptomatic ~P60 mice. Mice were first anesthetized using a mixture of Xylasin and ketamine. Next, 100 µL of Neurobasal containing X10 concentrated lenti-viruses ($6x10^9$ titer units), were

injected into the gastrocnemius muscles using a 1 mL syringe and a 25G needle. A pLL-miR126-5p-GFP construct was injected into the right hind foot, whereas a pLL-miR142-GFP construct was injected into the left hind foot. All animal experimentations were approved by the Tel-Aviv University Animal Ethics Committee.

Microfluidic chamber preparation

Polydimethylsilxane (PDMS) microfluidic chambers (MFC) were designed and cast as described previously (Ionescu et al., 2016). After the wells were punched, a small 'cave' was created in the explant well near the grooves using a 25G needle, keeping the explant in place. Microfluidic devices were cleaned of surface particles using adhesive tape and were sterilized in 70% ethanol for 15 minutes. Devices were completely dried under sterile conditions using UV radiation, and then attached to a sterile 60-mm plastic dish (Nunc) with gentle pressure, and the margins were sealed with PDMS before incubation at 70°C for 30 minutes to prevent the detachment of the chamber. Muscle channels were coated with Matrigel diluted 1:10 with DMEM containing 2.5% PSN for 30 minutes at 37°C, before filling the muscle wells with 150µL of Bioamf-2 medium. The explant well and channel were filled with 150µL of 1.5 ng/mL PLO (P-8638, Sigma) in PBS overnight, and then replaced with 150 µL laminin (L-2020, Sigma), 1:333 in deionized distilled water (DDW) overnight. One day before plating the spinal cord explant, laminin was replaced with explant medium containing Neurobasal (Life Technologies) supplemented with 2% B27 (Invitrogen), 1% penicillin-streptomycin (Biological Industries), 1% Glutamax (Life Technologies), 25 ng/mL brain-derived neurotrophic factor (Alomone Labs), until the day on which co-culturing began.

Fluorescence microscopy and image analysis

All confocal images were captured using a Nikon Ti microscope equipped with a Yokogawa CSU X-1 spinning disc and an Andor iXon897 EMCCD camera controlled by Andor IQ2 software. Epifluorescence was imaged using the same microscope in Bright field mode and images were captured with an Andor Neo sCMOS camera, or at a FLoid benchtop imaging station (Life Technologies). TIRF images were captured using a TILL photonics iMIC microscope (FEI Munich GmbH) with an Andor iXon897 EMCCD camera. All live-imaging assays were performed in a humidified 5% CO2 incubation chamber.

Western blotting

Muscle and sciatic nerve tissues of both sexes were excised and homogenized in lysis buffer containing PBS, 1% Triton X-100 (Sigma), and 1x protease inhibitors (Roche), followed by centrifugation and collection of the supernatant. Protein concentration was determined using the Bio-Rad Protein Assay. Protein samples were denatured by boiling in SDS sample buffer, which were then electrophoresed in 10% polyacrylamide gels (SDS-PAGE). Proteins were transferred to a nitrocellulose membrane and then immunoblotted with appropriate primary antibodies: Sema3A (Abcam, ab23393; 1:1000); NRP1 (Abcam, ab81321; 1:1,000); Sema3B (Abcam, ab48197; 1:2000); NRP2 (Cell signaling D39A5, 1: 1000) GFP (abcam ab13970 1:5000), (Tubulin 1:10,000; and ERK 1:10,000, diluted in 5% (w/v) Skim-milk (BD Difco) in TBS-T, followed by species-specific HRP-conjugated secondary antibodies (Jackson Laboratories 1:10000) and visualized using a myECL imager (Thermo), according to the manufacturer's instructions. Quantification was performed using ImageJ software.

Isolation and culture of hMSC

hMSC from healthy donors and ALS patients used in this study were obtained from bone marrow samples and were isolated, and then phenotypically characterized and cultured as described previously (Nachmany et al., 2012). All volunteers in this work signed a consent form before sample donation, according to the guidelines of the Hospital's Ethics Committee supervised by the Israeli Health Ministry Ethics Committee conforming with The Code of Ethics of the World Medical Association (Declaration of Helsinki), printed in the British Medical Journal (July 18,1964).

Motor neuron cell culture

Primary spinal cord neurons were cultured using E12.5 mouse embryos of either sex as previously described (Zahavi et al., 2015). Briefly, spinal cords were excised, trypsinized, and triturated. Supernatant was collected and centrifuged through a 4% BSA cushion. The pellet was re-suspended and centrifuged through an Optiprep gradient (10.4% Optiprep (Sigma-Aldrich), 10 mM Tricine, 4% glucose) for 20 min at 760 x g with the brake turned off. Cells were collected from the interface, washed once in complete medium, and then plated in coated growth chambers. Cells were maintained in Complete Neurobasal Medium (Gibco) containing B27 (Gibco), 10% (v/v) horse serum (Biological Industries), 25 nM beta-mercaptoethanol, 1% Penicillin-Streptomycin (PS; Biological Industries), and 1% GlutaMAX (Gibco) supplemented with 1 ng/mL Glial-Derived Neurotrophic Factor (GDNF), 0.5 ng/mL Ciliary

Neurotrophic Factor (CNTF), and 1 ng/mL Brain-Derived Neurotrophic Factor (BDNF), (Alomone Labs). Prior to plating, the growth plates were coated with 1.5 g/mL poly D-L-ornithine (PLO; Sigma-Aldrich) overnight at 37 °C and 3 g/mL Laminin (Sigma-Aldrich) for 2 hours at 37 °C. For immunofluorescence staining, 30,000 cells were plated on cover slides in 24-well plates. Cells were grown at 37 °C in 5% CO_2.

Spinal cord explants

Spinal cords were dissected from E11.5 mouse embryos of both sexes, either using HB9::GFP or SOD1^{G93A} stripped of meninges and dorsal root ganglia. The ventral horn was separated from the dorsal horn by longitudinal cuts along the spinal cord, and transverse sections up to 1 mm were placed in the explant well**.** Prior to plating, the growth chambers were coated with 1.5 g/mL PLO overnight at 37 °C and 3 g/mL Laminin overnight at 37 °C. Explants were maintained in Spinal Cord Explant Medium containing Neurobasal, 2% B27, 1% PS, and 1% GlutaMAX, supplemented with 25 ng/mL BDNF. Explants were grown at 37 °C in 5% CO_2.

Primary myocyte culture

Skeletal muscle cultures were derived from the gastrocnemius muscle of adult P60 female mice of either SOD1^{G93A} background or their LM using techniques previously described (Ionescu et al., 2016). Briefly, gastrocnemius muscles were excised and incubated in 2 mg/mL collagenase I (Sigma-Aldrich) in DMEM containing 2.5% penicillin-streptomycin-nystatin (PSN, Biological Industries) for 3 hours. Muscles were then dissociated and incubated for 3 days in Matrigel-coated (BD Biosciences) six-well plates with Bioamf-2 medium (Biological Industries) with 1% PSN at a density of ~120 myofibers per well. For purification of the myoblasts, adherent cells were trypsinized and pre-plated in an uncoated dish for 1 hr at 37°C. Non-adherent cells were then transferred into a Matrigel-coated dish with Bioamf-2 medium. Pre-plating was repeated for two days, keeping the culture at less than 50% confluence, before plating cells in MFC. Cultures were maintained at 37°C and in 5% CO_2. After the final pre-plating, 100,000 myocytes were cultured in the pre-coated distal compartment of the MFC. Myocyte Conditioned Media (CM) were produced as follows: At the final pre-plating stage, myoblasts were cultured in a Matrigel-coated 100 mm dish at 80% confluence and were incubated for 2 days with Bioamf-2 medium, followed by 2 days with rich DMEM (Biological Industries) medium containing 10% Fetal Calf Serum (Biological Industries), 10% Horse Serum (Biological Industries), 1% GlutaMAX, and 1% PSN. Then, once muscles reached a fully differentiated state, the culture dish was rinsed 3 times with pre-heated PBS and poor DMEM medium containing 1%

GlutaMAX and 1%PSN was applied on the cultures. CM was collected after 2 days, centrifuged for 5 minutes at 400 x g at 25°C, and streamed through a 0.22 µm PES filter.

CM preparation and application

Muscle myocytes of WT or SOD1^{G93A} mice were cultured as described before (Ionescu et al., 2016). Seven days after myocytes were fully differentiated, the muscles kept growing for 3 days in complete Neurobasal containing BDNF and GDNF. The conditioned media was refreshed with BDNF, GDNF, and Glucose after its collection, as described in (Nagai et al., 2007). Conditioned media under both conditions was applied on the axon compartment of the MFC for 48 hr.

Lentiviral vectors

Genes of interest were cloned into a third-generation lentiviral pLL3.7 backbone. HEK293T cells were transfected by employing calcium phosphate method and a mixture consisting of the vector of interest, vesicular stomatitis virus glycoprotein, and group antigens–polymerase (reverse transcriptase) was used. The medium was replaced after 5-8 hours, and the supernatant was collected 48 hours later. Next, 50 mM Hepes were added before freezing to maintain a neutral pH for long-term storage. When necessary, lentiviruses were concentrated using a PEG Virus Precipitation Kit (Abcam).

Neuromuscular junction staining

GC was excised from P60 mice and cleared of connective tissue, washed in PBS, fixed in 4% paraformaldehyde, washed once more, and then incubated with 1 g/mL Rhodamine Red-Conjugated Bungarotoxin (Sigma-Aldrich). Tissues were washed and then treated with methanol at -20 °C for 5 min, washed, and then blocked in blocking solution for 1 hour. Tissues were then rocked with appropriate primary antibodies diluted in blocking solution at room temperature overnight. Antibodies were used at the following concentrations: anti-Neurofilament Heavy Chain 1:500 (Abcam, ab72996; 1:1000; NFH) Synaptophysin (Millipore MAB5258 1:300) Synaptotagmin (Alomone ant-003 1:300); anti-NRP1 1:100; anti-Sema3A 1:100; anti-NRP2 1:100; anti-Sema3B 1:100. After having been washed, secondary antibodies (DyLight 405 anti-chicken 1:500; AlexaFluor 488 anti-chicken 1:500; AlexaFluor 647 anti-rabbit 1:500) were added for 4 hours at room temperature. Muscle fibers were spread into monolayers under a stereomicroscope and affixed to slides using VectaShield (Vector Laboratories). Cover slides were sealed with clear nail polish.

Quantification of myocyte contraction

1,000-frame-long movies of myocytes in the distal compartment of the microfluidic chamber were acquired 7 days post co-culturing. Imaging was performed under bright-field conditions at a rate of ~33 fps while using a 20X objective. A myocyte contraction plot was then profiled using an image-based method previously described (Zahavi et al., 2015; Ionescu et al., 2016). Briefly, only myocytes that came in contact with axons were plotted. Time-lapse images were taken for analysis using ImageJ. To create a time trace of contractions, high contrast (bright or dark) regions of interest (ROIs) were selected on each myotube. Movement of the selected spot due to myotube contraction was assessed by the change in the ROI intensity over time. The number of strong contractions, as measured from the time trace, was manually validated by re-examining the time-lapse image series. The number of strong and weak contractions in innervated myotubes was compared before and after 1μM TTX was added to the neuronal compartment. A myotube with a post to pre TTX difference of >50% was measured as an increase or decrease in contraction, and the fraction of increased, decreased, and unchanged myotubes was calculated.

Immunostaining of cell cultures

Cultures were fixed in 4% paraformaldehyde and permeabilized with 0.1% Triton X-100, 5% DS, 1 mg/mL BSA in PBS. Samples were blocked for 1 hour with blocking medium containing 5% DS, 1 mg/mL BSA in PBS. Primary antibodies against NFH (1:500), NRP1 (1:100), Sema3A (1:100), NRP2 (1:100), Sema3B (1:100), and Acetylated tubulin (1:1000), Ryanodine receptor 1 (Millipore AB9078 1:500), Alpha Actinin (Sigma A5044 1:400) Tau5 (abcam ab80579 1:500) MAP2 (Millipore ab5622 1:500) were diluted in blocking solution and incubated overnight at 4°C. Samples were incubated with species-specific fluorescent secondary antibodies for 2 hours at room temperature. DAPI was used for visualizing nuclei in myotubes. In MFC, after the staining protocol was completed, the MFC was peeled from the dish by gently pulling it from the proximal to the distal side. ProLong mounting medium was added and samples were covered with a #1.5, 18×18 mm cover-slide.

RNA extraction and cDNA synthesis

Muscle tissues were immediately frozen with liquid nitrogen. Tissue was ground to powder using a pestle and mortar. Then 700 μL of TriReagent (Sigma-Aldrich) were added to the muscle powder and the samples were further passed through a 21G needle 3 times for better homogenization. RNA from the TriReagent-rinsed samples

was further isolated following the TriReagent protocol. RNA quality was measured using NanoDrop3000 and a bio-analyzer. RNA purification of MN mass culture, along with transfected HeLa cells, was performed using TriReagent protocol as well. mRNAs were pooled in equal amounts and reverse transcribed into double-stranded cDNA by using the SuperScript2 kit (Qiagene).

NanoString Chip

One-hundred ng RNA samples were outsourced to NanoString technologies' facilities for a miR-Chip array assay of ~800 known miRs (Nanostring Technologies, Inc.). miR was quantified automatically by NanoString Technologies' instrumentation for miRs, which was hybridized with the template. Output data were analyzed by the nCounter analysis system. All miRs were normalized to the 100 most abundant miRs in the samples.

Primers design

Based on the consensus sequences of the desired transcripts, 2 sets of primers were designed for each gene (h – Human gene; m – Murine gene).

Gene	Forward Primer	Reverse Primer
hHPRT	GAACCAGGTTATGACCTTGATTTAT	GCAAGACGTTCAGTCCTGT
hSema3A	GCTCCAGTTATCATACCTTCCTTTTG	ACTGGCCACACAATCTTTTGAA
hNRP1	ACCTGTTCTCTTTCAGGGAA	CAAGTTGCAGGCTTGATTCG
hB2M	CCGTGTGAACCATGTGACTT	GGCATCTTCAAACCTCCATGA
hNRP2	GAGGCCAACCAGACCCA	CGTAAACAATCCACTCGCAGTT
hSema3B	TCTCCTTCCAAGTCCA	CTCGGCACCCACAAACA
mSema3A	CACTGGGATTGCCTGTCTT	GGCCAAGCCATTAAAAGTGA
mGFP	GCTACCCCGACCACATGAAGCA	GTCTTGTAGGTGCCGTCGTCCTTG
m-miR126	ID000451 (Thermo Fisher Scientific)	ID000451 (Thermo Fisher Scientific)

qPCR for mRNA detection

Quantitative Polymerase Chain Reaction (qPCR) was performed on the StepOne system (Life Technologies) in a 10 µL reaction containing 4 µL of RNA (20 ng), 5 µL Syber green master mix (Thermo Fisher Scientific), and 1 µL of reverse and forward primers.

miR vectors and transfection

Mammalian expression vector pMSCV-Blast-miR constructs were generously provided by Eran Hornstein from the Weizmann Institute of Science. Mammalian expression vector of C9orft72 Di-peptide PR_{50} and GR_{50} constructs were generously

provided by David Trotti from Jefferson University (Wen et al., 2014). Next, 50,000 HeLa / U87 human glioblastoma /muscles cells were plated in rich DMEM medium (1% PS, 1% GlutaMAX, 20% FBS). After 24 hours, the culture medium was replaced with serum-free medium (Opti-MEM) and cells were transfected using FuGene NE 6 (Promega) protocol. Cells were collected after 48 hours and used either for a functional assay or for RNA/protein extracts. Myocyte cultures were transfected using the same approach.

Semaphorin preparation

HEK293T cells were stably transfected to overexpress either Sema3A or an empty control. Conditioned media from 80% confluent cultures were collected after 3 days. We validated the purity level of the collected media using Coomassie staining and identified the stained band with a specific antibody against the desired protein using western blot analysis.

NRP1 antibody application

Five µg/ml NRP1 antibody (R&D System AF566 dot ETH0915031) for the extracellular domain was added to the distal compartment of the MFC while maintaining a proximal-to-distal volume gradient.

Histology tissue collection & fixation

Gastrocnemius muscles of 20 samples were harvested and fixed in 4% PFA. The samples were then outsourced for a histological assessment at Patho-Logica Company, Ness-Ziona, Israel. All tissues were trimmed into block cassettes and sent to CDX-Diagnostics for slide preparation.

Slide preparation & histological evaluation

Tissues were trimmed, embedded in paraffin sections at no more than 5 µm thickness and stained with Hematoxylin & Eosin (H&E). The mean minimal muscle fiber diameter thickness was measured in microns by performing a manual count using a 10X lens and analyzed by expert pathologist.

xCELLigence impedance measurement

For each experiment, 30,000 U87 cells were plated with rich DMEM medium in E-Plate L8 wells and incubated together with the xCELLigence system (ACEA Biosciences, Inc.) at 37°C, 5% CO_2 overnight. Impedance data were collected at 5-minute intervals. After 24 hours, poor DMEM medium (1% PS, 1% GlutaMAX) with

Sema3A or its control medium was replaced and recording proceeded. The data were analyzed using RTCA data analysis software 1.0 and normalized to the control sample.

CatWalk XT gait analysis

The Catwalk is a video-based analysis system used to assess gait in voluntarily walking mice (Noldus information technology). The principle of this method is based on an optical technique. The light of a fluorescence tube is completely internally reflected on a glass walkway floor. When the animal crosses the walkway, the light leaves the glass and illuminates only the area of contact. In this way, the different paw contacts are visualized. Based on position, pressure, and the surface area of each foot paw multiple parameters are calculated. Only compliant and continuing trials for each animal were analyzed, averaged, and the mean was calculated.

Experimental design and statistical analysis

Data are expressed as mean ± SEM. The statistical analysis was assessed by Student's *t*-test. In all cases, differences were considered to be statistically significant if $p < 0.05$. Symbols are as follows: *: P<0.05, **: P<0.001, ***: P<0.0001.

Results

Sema3A and NRP1 levels are elevated in muscles and the MNs of ALS models

ALS disease is considered to be a distal axonopathy involving axon degeneration and NMJ disruption as a key processes in its pathology (Fischer et al., 2004). We therefore hypothesized that destabilizing factors secreted from adult pre-symptomatic ALS mutant muscles might be involved in triggering axon degeneration of MNs. Since Sema3A is known to act in such a manner, at least in development, and it was already reported to be elevated in ALS, we decided to focus on this factor (De Winter et al., 2006; Körner et al., 2016). Following this hypothesis, we first examined the expression of Sema3A in $SOD1^{G93A}$ gastrocnemius (GC) muscles in comparison with that of their littermates (LM); (Figure 1 A-B; Figure 1-1). Western blot analysis of muscle protein extracts revealed significant elevations in Sema3A protein levels in muscles of pre-symptomatic $SOD1^{G93A}$ mice as early as P30 and P60, whereas testing Sema3A levels in younger animals (P7) showed no apparent differences compared with their LM controls (mean fold change over LM: P30 $SOD1^{G93A}$ 3.08 ± 0.86; P30 LM 1 ± 0.36; P60 $SOD1^{G93A}$ 2.2 ± 0.45; P60 LM 1 ± 0.32; P7 $SOD1^{G93A}$: 1.2 ± 0.7; P7 LM: 1 ± 0.42). In order to validate this difference, we also tested the transcript levels of Sema3A (Figure 1 C). Quantitative PCR analysis of total RNA

extracts from muscles at pre symptomatic SOD1^{G93A} stage and LM mice identified a ~1.7-fold increase in Sema3A mRNA of SOD1^{G93A} muscles (mean fold change over LM: SOD1^{G93A} 1.72 ± 0.32; LM 1 ± 0.06). Since GC muscle tissues contain heterogeneous cell types and in order to verify that the levels of Sema3A are indeed higher specifically in SOD1^{G93A} muscles fibers, we immunostained primary myocyte cultures from P60 SOD1^{G93A} and LM mice for Sema3A (Figure 1 D-E). Quantifying the mean intensity values showed a significant 50% increase in the SOD1^{G93A} myocytes (a mean fold change in intensity over LM: SOD1^{G93A} 1.5 ± 0.06; LM 1 ± 0.04). We also collected conditioned media (CM) from myocyte cultures to determine whether the increase in Sema3A protein also results in an increase in its secretion (Figure 1 F). Western blot analysis indicated that Sema3A levels were also elevated in P60 SOD1^{G93A} myocyte-conditioned media (a mean fold change over LM: SOD1^{G93A} 2.3± 0.55; LM 1 ± 0.08). Because NMJ disruption is a primary event in ALS, we sought to examine the levels of Sema3A in NMJ *in vivo* (Figure 1 G-H). Immunostaining for Sema3A in GC muscles showed a 6-fold increase in the number of muscle fibers expressing Sema3A in their NMJs. Whereas only ~5% of NMJs stained positively for Sema3A in LM muscles, we identified its expression in ~30% of NMJs in P60 SOD1^{G93A} mice (the mean percentage of NMJs expressing Sema3A: SOD1^{G93A} 30.83% ± 4.73%; LM 4.56% ± 2.4%). Interestingly, a previous study described Sema3A elevation in SOD^{G93A} mice specifically in fast fatigue NMJs expressing myosin-IIb marker (De Winter et al., 2006). Since fast fatigue NMJs are the first to become disrupted and be eliminated in ALS pathology, we examined Sema3A levels both at P90 and P120 and hypothesized that Sema3A levels will eventually drop in later stages of the disease. We found that whereas the percentage of NMJs expressing Sema3A in SOD^{G93A} in P90 animals is similar to P60, the end stage animals (P120) were shown to display a reduction in Sema3A-positive NMJs and no apparent difference existed between WT and SOD1^{G93A} mice (Figure 1-2 A-B). Taken together, these results indicate that a significant part of the MN population is exposed to high levels of Sema3A in pre-symptomatic stages and that this specific population is disrupted and eliminated during disease progression. We then proceeded to investigate the expression of the Sema3A-receptor binding unit, NRP1, in ALS (Figure 1 I). Western blot analysis of GC muscle extracts revealed a significant ~8-fold increase in NRP1 (the mean fold change over LM: SOD1^{G93A} 8.6 ± 2.2; LM 1 ± 0.3). Since MNs are a primary target in ALS, we wanted to determine whether NRP1 is also overexpressed in the MNs of SOD1^{G93A} mice. First, we performed western blot analysis of sciatic nerves (SNs) and observed a ~2-fold elevation in NRP1 levels of P60 SOD1^{G93A} mice (Figure 1 J; the mean fold change

over LM: $SOD1^{G93A}$ 1.96 ± 1.22; LM 1 ± 0.21). Next, we obtained protein extracts of primary MN cultures for western blot analysis and confirmed a ~2.5-fold elevation in NRP1 levels in the MNs of $SOD1^{G93A}$ culture (Figure 1 K; the mean fold change over LM: $SOD1^{G93A}$ 2.3 ± 0.16; LM 1 ± 0.06). Immunostaining of primary MN cultures for NRP1 resulted in analogous findings (Figure 1 L-N). Intriguingly, the NRP1 signal in $SOD1^{G93A}$ is generally higher than in LM, and is increased even more in axons compared with cell bodies (the mean fold change over LM: $SOD1^{G93A}$ soma 1.86 ± 0.13; LM soma 1 ± 0.05; $SOD1^{G93A}$ axon 3.83 ± 0.95; LM axon 1 ± 0.11). Finally, immunostaining for NRP1 in GC muscles confirmed a similar shift of ~30% in the number of NMJs expressing NRP1, as we had observed for Sema3A in $SOD1^{G93A}$ mice, both at P60 and P90. However, also this time the differences were abolished in the end stages of the disease (P120) (Figure 1 O-P, Figure 1-2 C-D; the mean percentage of NMJs expressing NRP1: P60: $SOD1^{G93A}$ 27.5% ± 2.04%; LM 21.27% ± 1.22%). In order to determine whether the elevated NRP1 levels result from feedback due to an increase in its ligand, we treated primary MN cultures from LM embryos with soluble Sema3A for 3 days and performed western blot analysis on cell culture lysates. Importantly, we did not observe any difference in NRP1 expression after applying Sema3A, suggesting that NRP1 levels are regulated by an intrinsic mechanism in MNs (Figure 1-3). Finally, to validate our finding with other ALS models and to emphasize the impact of Sema3A in ALS, we performed western blot analysis for Sema3A and NRP1 expression in human mesenchymal stem cells from sporadic ALS patients and healthy controls, as well as in myocyte-expressing C9orf72-PR_{50} and their conditioned media for Sema3A. In addition, we compared the results with those of a mock control. Remarkably, in all of these ALS models, we identified high expression of Sema3A and NRP1 (Figure 1-4).

Taken together, our combined *in vivo* and *in vitro* data suggest that the levels of both Sema3A and its co-binding receptor, NRP1, are pre-symptomatically increased in several ALS models as well as in sALS patients. These findings suggest that the Sema3A pathway is a common denominator in various ALS mutations and thus, it may contribute to MN degeneration in ALS.

Application of Sema3A on wild-type MN axons results in axon degeneration

Since our findings suggest that Sema3A is produced and secreted in excess from muscles of ALS models, and since muscles interact specifically with MN axons, we sought to test the activity of Sema3A exclusively in this distal subcellular compartment. To this end, we utilized a microfluidic chamber (MFC) that allows

precise control, monitoring, and manipulation of subcellular microenvironments (Figure 2-1) (Zahavi et al. 2015). We cultured healthy ventral spinal cord (SC) explants from transgenic mouse embryos expressing GFP under the MN-specific promoter HB9 (HB9::GFP) in one compartment of the MFC and enabled axons to extend into the opposing compartment, thus segregating axons and cell bodies into two isolated compartments. In order to verify that our MFCs can efficiently segregate MN axons from their somata, we stained the neuronal culture in the MFC system for the dendritic and axonal markers MAP2 and Tau, respectively (Figure 2-1). We confirmed that all neurites that traversed the distal compartment are positive for Tau staining and negative for MAP2. Next, we purified Sema3A or control media as described before (Ben-Zvi et al., 2006), and applied them to the distal compartment, while imaging the axons for 16 hours (Figure 2 A). Our recordings reveal extensive axon degeneration in the Sema3A-treated MFCs 6-8 hours after its application (Figure 2 B; Movies 1-2) (the mean percentage of degenerated axons: Sema3A 83.01% ± 3.54%; control 23.94% ± 7.6%). Co-application of NRP1-blocking antibody and Sema3A on MN axons inhibits the Sema3A-dependent axon degeneration (Figure 2 B; the mean percentage of degenerated axons: Sema3A and NRP1 antibody 25.00% ± 12%). These data indicate that Sema3A can trigger axon degeneration in MNs when applied exclusively on distal axons, and further support our hypothesis that an increase in muscle-derived Sema3A might contribute to axon degeneration in ALS.

Muscles expressing diverse ALS mutations initiate axon degeneration

In order to study the molecular mechanisms enabling the communication between MNs and their environment, which are essential for cell survival and synapse maintenance, we extended the use of the MFC system to co-culture primary MNs and primary myocytes (Ionescu et al., 2016). Briefly, ventral spinal cord (SC) explants from healthy 12-day-old (E12) HB9::GFP embryos were cultured in the proximal compartment, in the presence or absence of primary myocytes extracted from adult mice in the distal compartment (Figure 2-1). As we showed before (Zahavi et al., 2015), culturing HB9::GFP explants in the presence of wild-type muscles facilitates the rapid and directed growth of axons into the distal compartment (Figure 2-1), suggesting that muscles secrete factors that support and promote the growth of motor axons. However, since ALS-mutated muscles were found to have intrinsic abnormalities throughout disease progression (Loeffler et al., 2016), we hypothesized that the nature of these factors will be altered. In order to study the effect of ALS muscles on MN axons in a simplified system, we plated primary myocytes from pre-

symptomatic P60 $SOD1^{G93A}$ and LM mice as well as WT myocytes transfected to express $SOD1^{wt}$ in the distal compartment. Myocyte cultures were allowed to fuse and differentiate. Importantly, in all the described cases myocyte morphology, fusion, and differentiation parameters were similar, and the culture showed no apparent difference (Figure 2-2). After 7 days, HB9::GFP Spinal Cord (SC) explants were cultured in the proximal compartment. Co-cultures were incubated until the HB9::GFP axons began extending toward the microgroove compartment. Once the axons reached the microgroove compartment, the extension of HB9::GFP axons along the microgrooves was recorded for 16 hours (Figure 2 C). Surprisingly, HB9::GFP axons that were co-cultured with the $SOD1^{G93A}$ myocytes were less likely to traverse the distal side (Figure 2 D-E). During this period, axons extending towards the $SOD1^{G93A}$ myocytes were markedly incapable of traversing the distal compartment and underwent retraction, degeneration, or remained static in place, as compared with the LM and $SOD1^{wt}$ controls (Figure 2 D, movies 3-4). Noteworthy, the addition of NRP1-blocking antibodies to the distal compartment, targeting Sema3A binding to the extracellular site of NRP1, improved the traversing rate of axons (Figure 2 E; the mean axon traversal rate per field: LM 33.88% ± 10.40; $SOD1^{wt}$ 52.66% ± 12.7% $SOD1^{G93A}$ 11.1% ± 5.5%; $SOD1^{G93A+NRP1\text{-}ab}$ 28.18 % ± 5.4 %). We further transfected primary myocyte cultures with several more ALS-linked mutations or aberrant toxic proteins as follows: C9orf72-PR_{50}, C9orf72-GR_{50} (Wen et al., 2014), and $TDP43^{A315T}$ and used empty-GFP vector as a control. Transfected myocytes exhibit normal morphology and fusion in comparison with the WT muscle culture in our system (Figure 2-2). Nevertheless, all ALS-causing mutations that we examined recapitulated the phenotypes we described previously in $SOD1^{G93A}$ (Figure 2 F; GFP 40.65% ± 16%; GR_{50} 5.2% ± 3.49%; PR_{50} 0 ± 0 %; $TDP43^{A315T}$ 8.75% ± 6.39%). These results suggest that the dysregulated secretion of factors from ALS mutant muscles takes place, which in turn, activates axon retraction and degeneration. Because muscles can either secrete positive or negative signaling molecules, we could not determine whether our observation within this assay originates from an increase in the release of destabilizing factors or the diminished release of positive factors. To this end, we collected muscle-conditioned media from WT and $SOD1^{G93A}$ muscle cultures in complete medium containing positive factors such as BDNF and GDNF, as was previously performed in mass culture (Nagai et al., 2007), and ultimately applied it only to the distal axons of both WT and $SOD1^{G93A}$ MNs (Figure 2 G-H). Interestingly, we observed that axon degeneration occurs only when $SOD1^{G93A}$ myocyte-conditioned media is applied to $SOD1^{G93A}$ axons (Figure 2 H; LM 3.72% ± 1.15%; $SOD1^{G93A}$ 34.7% ± 4%), whereas in all other combinations the

axons remained intact (Figure 2-3). To further determine whether type 3 semaphorins such as Sema3A contribute to MN axon degeneration in this assay, we investigated whether NRP1-blocking antibody application can block this phenotype. Here again, we observed a rescue effect by this treatment (Figure 2 H, $SOD1^{G93A}$ + NRP1-antibody 18.6% ± 7%), although the protection was incomplete. These results reinforce our hypothesis, suggesting that ALS-mutated muscles secrete destabilizing factors such as Sema3A. Importantly, these results emphasize that $SOD1^{G93A}$ MNs exhibit a higher sensitivity to degeneration, and support the MN unique vulnerability as well as the non-cell autonomous mechanism of ALS. Interestingly, previous attempts to block Sema3A signaling in $SOD1^{G93A}$ mice using either a similar antibody approach or by crossing transgenic mice expressing a truncated form of Sema3A with $SOD1^{G93A}$ mice also resulted in only a mild improvement or none at all of motor functions (Venkova et al., 2014; Moloney et al., 2017). This suggests that Sema3A plays a complex role in MNs and that perhaps other related proteins are involved. This also led us to investigate whether a wider deregulation of secreted factors released by the diseased muscles exists. Indeed, examining other members of the Semaphorin family, we found that the percentage of NMJs expressing Sema3B, as well as NRP2 is elevated in the $SOD1^{G93A}$ ALS model (Figure 2-4). Therefore, we concluded that the destabilizing effect of ALS muscles over MN axons involves more than a single factor, and thus it cannot be blocked or rescued by targeting one factor at a time. Moreover, the multiplicity of effectors suggests that a higher-order regulator such as miRNA might be involved in this process.

miR126-5p is down-regulated in ALS models and modulates Sema3A, Sema3B, NRP1, and NRP2 protein expression levels

In order to identify the mechanism underlying the elevated levels of various secreted destabilizing factors in muscles of ALS models, we scanned for alterations in miRNAs (mIRs) that can regulate the expression of multiple proteins. miRs have been previously linked to MN toxicity in ALS (Haramati et al., 2010). We used Nanostring miRNA-chip technology to screen for alterations in ~800 miRs of pre-symptomatic P60 $SOD1^{G93A}$ mice and their LM controls. The screen yielded 8 significantly altered miRs (Figure 3 A, Figure 3-1). Since we found that Sema3A levels were elevated in muscles, we narrowed our focus to those miRs that were reduced and that could regulate its expression, specifically miR126-5p and miR133a (Figure 3 B; the mean fold change over LM: $SOD1^{G93A}$ 0.74 ± 0.03; LM 1 ± 0.03, Figure 3-1). A targeted search for these miRs in databases (miRDB, Pictar, miRbase, and miRTarBase) revealed that both miRs are predicted to regulate Semaphorin

signaling genes as well as other relevant transcripts of ALS-related genes. Interestingly, we previously described deep-sequencing analyses of primary MN cultures expressing $SOD1^{G93A}$ or $TDP43^{A315T}$ and demonstrated that miR126-5p is also correspondingly decreased in diseased MN axons, but not in the their soma (Rotem et al., 2017). This information led us to further focus our investigation on miR126-5p. We used qPCR to validate that miR-126-5p levels in $SOD1^{G93A}$ GC muscles point to a similar trend (Figure 3 C; the mean fold change over LM: $SOD1^{G93A}$ 0.47 ± 0.2; LM 1 ± 0.45). In order to verify that miR126-5p can regulate the expression of Semaphorin3 and Neuropilin signaling members, we transfected HeLa cells, which are known to endogenously express Sema3A, Sema3B, NRP1, and NRP2 (Fujita et al., 2001), with miR126-5p or with the irrelevant miR142, which is not predicted to target any of these genes, as a negative control. To this end, we isolated RNA from these cultures and performed qPCR analysis to determine the mRNA levels of Sema3A, Sema3B, NRP1, and NRP2 (Figure 3 D-G). Our results indicate that miR126-5p specifically targets Sema3A, NRP1, Sema3B, and NRP2 (RT-PCR: mean ΔCt-NRP1: miR126 3.79 ± 0.71; miR142 2.83 ± 0.57; ΔCt-Sema3A: miR126 4.84 ± 0.22; miR142 3.84 ± 0.34; ΔCt-NRP2: miR126 7.6 ± 0.30; miR142 6.2 ± 0.37; ΔCt-Sema3B: miR126 8.1 ± 0.10; miR142 7.05 ± 0.14). To investigate whether miR126-5p overexpression can also inhibit Sema3A function, we used a recently described impedance-based approach. U87MG human glioblastoma cells, which express NRP1 (Figure 3-2 A) and were used previously specifically in this assay (Birger et al., 2015), were transfected to overexpress miR126-5p or miR142 as a control. One day after transfection, cells were re-suspended and plated in xCELLigence multiwell electric plates. The next day, Sema3A was added to the cultures and any morphological or adhesive changes were monitored by the impedance readout. As demonstrated by TIRF imaging (Figure 3 H), adding Sema3A to responsive cells, such as U87MG cells, induces their detachment from the culture dish. This detachment can be measured as a decrease in impedance (Figure 3-2 B). Shortly after Sema3A was added to the cultures, cells expressing miR142 exhibited decreased impedance, whereas cells expressing miR126-5p did not respond to Sema3A in the medium and kept growing with a corresponding increase in impedance (Figure 3 I). Hence, we showed that the excess production of destabilizing factors in ALS is likely to be mediated downstream of a deregulation in miR126-5p.

Overexpression of miR126-5p can block $SOD1^{G93A}$ muscle toxicity

We overexpressed miR126-5p in SOD^{G93A} myocyte cultures and quantified Sema3A levels in their culture extract as well as in their conditioned media. Western blot analysis indicated that Sema3A levels in both the culture extract and conditioned media are depleted, compared with miR142 (Figure 4 A-B; the mean fold change over $SOD1^{miR142}$: Muscle extract - $SOD1^{miR126}$ 0.24 ± 0.1; $SOD1^{miR142}$ 1 ± 0.4 Muscle-conditioned media - $SOD1^{miR126}$ 0.63 ± 0.03; $SOD1^{miR142}$ 1 ± 0.13). Next, we investigated whether overexpressing miR126-5p in both $SOD1^{G93A}$ and PR_{50} myocytes can rescue the negative effect on MN growth that we observed before. To this end, primary myoblasts were transfected to overexpress either miR126-5p ($SOD1^{miR126}$; PR_{50}^{miR126}) or miR142 ($SOD1^{miR142}$; PR_{50}^{miR142}), and were then plated in the distal compartment of the MFC. Myoblasts were differentiated into mature myocytes while expressing the miRs for 7 days, after which HB9::GFP explants were cultured in the proximal compartment. Once axons reached the microgrooves, their extension toward the muscle compartment was monitored for 16 hours (Figure 4 C). Evidently, co-cultures with $SOD1^{miR126}$ and PR_{50}^{miR126} myocytes retained wild-type behavior and manifested a clear rescue effect on the rate of axon traversal (Figure 4 D-E; the mean traversal rate of axons: $SOD1^{miR126}$: 40.77% ± 6.68%; $SOD1^{miR142}$ 12% ± 7.6%; PR_{50}^{miR126}: 45.6% ± 9.4%; $PR50^{miR142}$ 16% ± 3.6%). Thus far, we have shown that myocytes expressing various ALS-linked mutations facilitate MN axon degeneration and delay their growth in a simplified compartmental co-culture assay. However, while observing the co-cultures for longer periods, we found that axons eventually do traverse the muscle compartment and form functional synapses with the myocytes. Using an image-based method that we recently developed to quantify contraction and assess the innervation in *in vitro* co-cultures (Ionescu et al., 2016; Zahavi et al., 2017), we observed that the contractile behavior of innervated $SOD1^{G93A}$ myocytes is significantly different from that of innervated LM myocytes, which tend to contract in a bursting pattern (Figure 4 F-G, movies 5-6). Whereas 37% of innervated myocytes contract in a bursting pattern, only 18% of the innervated $SOD1^{G93A}$ myocytes contract in this pattern (the mean rate of bursting innervated myocytes: LM 37.23% ± 2.8%; $SOD1^{G93A}$ 18.5% ± 2.03%). Strikingly, $SOD1^{miR126}$ myocytes retain the same rate of bursting myocytes as the LM myocytes (Figure 4 G; the mean rate of bursting innervated myocytes: $SOD1^{miR126}$ 37.66% ± 4.29%; $SOD1^{miR142}$ 26.26% ± 0.59%). Hence, miR126-5p is an effective regulator of muscle-secreted factors such as Sema3, and can rescue the detrimental effect of destabilizing factors on MN axons, as well as on NMJ function and maintenance *in vitro*.

miR126-5p transiently rescues early motor phenotypes of SOD1^{G93A} mice *in vivo*

NMJ disruption, muscle morphology abnormalities, and Hind-limb misprints are major phenotypes in SOD1^{G93A} mice (Gurney et al., 1994). To determine whether miR126-5p can moderate those phenotypes, we injected SOD1^{G93A} mice with either pLL-eGFP-miR126 (SOD1^{miR126}) or pLL-eGFP-miR142 (SOD1^{miR142}) into the right and left GC muscles of pre-symptomatic mice (P60), respectively (Figure 5 A). Virus expression was validated both *in vitro* on MNs and in muscle cultures (Figure 5-1 A) as well as *in vivo* at the transcript and protein levels (Figure 5-1 B-C). Importantly, we observed a decrease in the number of NMJs expressing Sema3A in the pLL-eGFP-miR126-5p-injected gastrocnemius muscles in comparison with the miR142 group, suggesting that miR-126-5p is active in the injected tissue (Figure 5-1 D). Next, we performed a series of histological analyses, followed by motor behavioral tests at two time points post injection: at the age at which mice typically begin exhibiting ALS phenotypes (P90) as well as in the disease end stage (P120) (Fischer et al., 2004). Since NMJ disruption is a key process in ALS, we sought to determine whether overexpression of miR126-5p results in reduced NMJ disruption. Briefly, both the left and right GC muscles were fixed and stained for synaptic markers of the NMJ (Figure 5 B). Quantifying the percentage of intact NMJs at P90 injected mice revealed a significantly higher innervation rate in miR126-5p expressing muscles compared to both mock-treated and to SOD1^{G93A} muscles (Figure 5 C; P90: WT 71.58% ± 3.32; SOD^{G93A} 42.58% ± 2.64; SOD1^{miR126} 64.25% ± 5.8; SOD1^{miR142} 46.54% ± 7.2). Furthermore, careful analysis at P120 also identified a mild rescue by miR-126-5p overexpression. (Figure 5 C; P120: WT 74.35% ± 4.74; SOD^{G93A} 20.12% ± 5.01; SOD1^{miR126} 30.82% ± 3.97; SOD1^{miR142} 18.18% ± 3.12). Next, we performed histological analyses to determine muscle fiber wasting and tissue abnormalities (Figure 5 D-E). P120 Gastrocnemius muscles of WT, SOD1^{G93A}, and both SOD1^{miR126} and SOD1^{miR142} were stained with H&E for histological examination and the minimal diameter of myofibers was analyzed as described in material and method section. We observed a mild, but significant, increase in the minimal fiber size of the SOD1^{miR126}-injected muscle compared to the SOD1^{miR142} mock control, (Figure 5 C; P120: WT 40.25% ± 2.28; SOD^{G93A} 18.5% ± 0.64; SOD1^{miR126} 23± 1.87; SOD1^{miR142} 19 ± 1.47). Lastly, we performed a behavioral test using the CatWalk Gait Analysis technique. This video-based method is a computerized version of the ink bath assay and provides an objective and dynamic wide range of gait analyses (Deumens et al., 2007). Moreover, it has been used before specifically with the SOD1^{G93A} mouse

model and displayed significant differences in several parameters (Mead et al., 2011; Gerber et al., 2012)(Figure 5 F). One output is the Mean Stand Index (MSI), which measures the speed at which the paws detach from the walking surface. Since aged $SOD1^{G93A}$ mice suffer motor defects, their MSI values for both hind limbs are dramatically lower than their LM values. Remarkably, the MSI values of the $SOD1^{miR126}$-injected limbs were significantly higher at P90 and similar to the LM control values, whereas the $SOD1^{miR142}$-injected limb was reminiscent of typical $SOD1^{G93A}$ behavior (Figure 5 G) (the mean fold change over WT: $SOD1^{G93A}$ 0.68 ± 0.02; $SOD1^{miR126}$ 0.74±0.06; $SOD1^{miR142}$ 0.65 ± 0.04; LM 1 ± 0.04). We also examined other established parameters that have been shown to be altered in the SOD^{G93A} model (Mead et al., 2011). We specifically focused on the percentage of single support parameter, which indicates the relative duration of contact of all combined paws with the glass floor, and on the base of support parameter, which indicates the average width of limb spreading between both front, or both hind paws. Remarkably, we observed a significant rescue phenotype for both parameters in the injected mice at age of P90. Furthermore, the improvement in base of support parameter persisted also in P120. (Figure 5 H-I) (Percent of Support Single: $SOD1^{G93A}$ 0.43 ± 0.05; Injected 1.06 ± 0.24; LM 1 ± 0.1; Base of Support, P90: $SOD1^{G93A}$ 0.87 ± 0.01; injected 1.02 ± 0.02; LM 1 ± 0.02; P120: $SOD1^{G93A}$ 0.858 ± 0.02; injected 0.95 ± 0.02; LM 1 ± 0.02).

Taken together, we demonstrated *in vivo* that miR126-5p reduces the detrimental effects of muscle-secreted destabilizing factors such as Sema3A on MN axons and motor function in ALS models.

Discussion

In this work, we demonstrated that the muscle toxicity in ALS is mediated by miR126-5p. We provided one specific mechanism for a well-described molecule (Sema3A), by which miR126-5p contributes to ALS pathology. We have also demonstrated that miR126-5p alterations facilitate axon degeneration and NMJ disruption in an ALS model as an outcome of pre-symptomatic elevations in the production and secretion of their target genes, which encode for destabilizing factors such as Sema3 family members. Overexpressing miR126-5p in $SOD1^{G93A}$ muscles inhibits the neurodegenerative process. These findings reveal how alterations in miR126-5p can be toxic to MNs, and identify a non-cell autonomous neurodegeneration process in ALS (Figure 6).

miR126-5p as a master regulator of proper NMJ function

Our results indicate that the expression of ALS–causative mutations results in the secretion of repellent factors including a number of type 3 Semaphorins and potentially other factors. It is thus likely that a general gene repression mechanism, specifically miR system, is altered under such conditions. This assumption is also consistent with the fact that miR alterations are apparent in various neurodegenerative diseases including ALS (Haramati et al., 2010). Here we identified such a miR and showed how alterations in this specific miR can regulate the essential signaling pathways in MNs and can trigger neurodegeneration. Intriguingly, and in line with our finding, a very recent paper demonstrated a mechanism by which miR126-5p modulates Sema3A expression through SetD5 expression and it emphasizes its positive effect on retinal endothelial cells' survival (Villain et al., 2017). However, aside from targeting Sema3A and Sema3B, as well as NRP1 and NRP2, miR126-5p is predicted to regulate other Semaphorin signaling factors such as Sema6D, PLXNA2, JNK2, JNK3, and PTEN. In addition, miR126-5p can regulate the ALS and motor-unit-related genes VEGF-A, SPAST, MMPs (Kaplan et al., 2014), AGRIN (Vilmont et al., 2016), and C9orf72, which are directly involved in ALS. Therefore, miR126-5p can serve as a master regulator of NMJ health by controlling multiple signaling pathways.

Sema3 alterations in ALS – Settling the contradictory reports

A critical initiating event for the mechanism outlined above is the alterations in Sema3 signaling in ALS models and patients. Sema3 family members were previously found to be up-regulated in terminal Schwann cells (TSCs) in the NMJs of $SOD1^{G93A}$ mice (De Winter et al., 2006). Recently, Sema3A was also shown to be elevated in the motor cortex of post mortem ALS patients but not in their spinal cord (Körner et al., 2016). Consistent with this, NRP1-antibodies, blocking the obligatory binding receptor for Sema3A, were injected into $SOD1^{G93A}$ mice as a potential treatment (Venkova et al., 2014). However, anti-NRP1 blocking antibody had only a modest effect. Moreover, a recent study demonstrated that crossing mice expressing a truncated form of Sema3A with $SOD1^{G93A}$ mice did not result in any rescue effect (Moloney et al., 2017). An explanation for a minor effect or not at all, as a result of blocking Sema3A activity, could be based on the idea of multiple toxic factors that play a role in ALS pathology. Another explanation for this contradiction could be the fact that Sema3A plays a more complex role in the biology of MNs. Indeed, Sema3A was shown to increase survival when added to mass cultures of mouse MNs

(Molofsky et al., 2014), and human MNs (Birger et al., 2018). Consistent with this, deletion of the Sema3A gene specifically in spinal astrocytes resulted in a gradual loss of spinal MNs (Molofsky et al., 2014), thus, suggesting that Sema3A has a positive effect when introduced near the cell body. When these findings are taken together with our results, apparently Sema3A has both positive and negative effects on MNs, perhaps depending on its specific subcellular localization. When Sema3A is secreted from muscles and targets distal axons at NMJs, it mediates their destabilization; however, when it is secreted by spinal astrocytes and targets MN soma, it acts as a survival factor. Thus, it is perhaps not surprising that a genetic approach to inhibit Sema3A in all cells in a mouse model of ALS had no effect in inhibiting the symptoms. The injection of anti-NRP1 may have been a bit more beneficial possibly either because it was able to inhibit Sema3A outside the CNS more effectively, or alternatively, because NRP1 blocks other type 3 semaphorins as well.

Autonomous versus non-cell autonomous contributions to ALS progression

ALS is considered a complex disease, with unique MN features as well as a non-cell autonomous contributions (Ilieva et al., 2009; Musarò, 2013). Some evidence suggests that the NMJ is the first compartment to be disrupted in ALS rather than the MN soma; the disease is recognized as distal axonopathy in a non-cell autonomous process (Fischer et al., 2004; Moloney et al., 2014). Two main cell populations that have been shown to play a role in distal axonopathy are glia and muscle cells, which secrete factors that influence MN survival and health (Moloney et al., 2014; Tsitkanou et al., 2016). However, the complexity of the disease and the involvement of several tissues raise controversies regarding the contribution of each tissue to the disease pathology. With skeletal muscle, few works have concluded that muscles do not play a role in ALS pathology. Reducing $hSOD^{G93A}$ levels by injecting siRNA against its transcript directly into muscles of the SOD^{G93A} mouse model, as well as crossing Lox SOD^{G37R} with the Cre coding sequence under the control of the muscle creatine kinase (MCK) promoter, or performing manipulations using Follistatin did not affect the disease onset and survival (Miller et al., 2006). *In vitro* application of muscle-conditioned media from SOD^{G93A}-expressing muscle on healthy mass culture and ES cell-derived motor neurons resulted in no effect (Nagai et al., 2007). However, in contrast with these findings, evidence indicates that overexpressing mutant SOD1 protein specifically in healthy skeletal muscle induces an ALS phenotype and the degeneration of MNs, supporting a direct role for muscle in ALS physiology

(Dobrowolny et al., 2008; Wong and Martin, 2010). Moreover, muscle from ALS patients and models have been shown to exhibit impaired mitochondrial function (Shi et al., 2010) and abnormalities in muscle biology (Manzano et al., 2012). Here, we demonstrated that applying pre-symptomatic $SOD1^{G93A}$ muscle-conditioned media directly, and only on $SOD1^{G93A}$-expressing MN axon tips results in their degeneration, suggesting that both tissue types are necessary for exhibiting the disease phenotype. Furthermore, contradictory reports were published on transgenic mice expressing $SOD1^{G93A}$ only in the MNs. For example, Lino et al. showed a very mild phenotype, whereas Jaarsma et al. demonstrated a significant toxic effect (Lino et al., 2002; Jaarsma et al., 2008). In this study, we showed that muscle-secreted factors are capable of modulating MN axons. Whereas wild-type muscle-secreted factors facilitate axon growth, several ALS-related mutations, expressed in muscles, result in the secretion of factors that cause retraction and degeneration when exclusively introduced to axons. At least one of these factors is Sema3A. The secretion of Sema3A by the muscle itself is likely to contribute to the instability of the MN axons. However, our results also show that ALS mutant muscles themselves cause axon degeneration and a delay in axon growth towards the muscles, but eventually, the connections between axons and muscles are established. Thus, at least in our system, apparently the non-cell autonomous contributions of the muscle are insufficient to recapitulate all the toxic effects on MNs. However, once the MNs also carry an ALS mutation, axons are more susceptible to degeneration by mutated muscle-conditioned media (Figure 3 G-H), thus demonstrating the critical contribution of the MNs to ALS progression.

Do diseased muscles initiate axon degeneration or inhibit regeneration?

Our data suggest that muscles are involved in modulating MN health in ALS disease. We showed, both *in vivo* and *in vitro,* that muscles secrete destabilizing factors such as Sema3A, as well as facilitate axon degeneration and NMJ disruption. Intriguingly, a previous study demonstrated that Sema3A expression is limited only to myosin IIb positive fibers, which are prone to be disrupted first in ALS (De Winter et al., 2006). These data support our findings in which the percentage of NMJs that express Sema3A and NRP1 is reduced at the end stage of the disease, most likely along with the fast fatigue NMJs. However, although the suggested mechanism involves muscle-MN interaction, owing to the nature of our experimental model, we cannot fully determine whether the mutated muscles act by initiating the degeneration of MN axons or by inhibiting their regrowth and NMJ repair, which was also suggested

before (Arbour et al., 2015). Perhaps muscle toxicity plays an active role in both pathways. However, future efforts should be made to resolve this issue.

miRs as a potential therapeutic strategy for ALS disease

In this paper, we demonstrated a positive effect of miR126-5p on ALS disease progression and suggested a potential therapeutic strategy for ALS disease. Nevertheless, our *in vivo* data show that the most significant positive effect of miR126-5p on ALS pathology was achieved at P90, whereas at later stages only modest effects were achieved. These results point to miR126-5p as a targeted treatment for an early phenotype but without a sustained beneficial contribution at later stages of ALS disease. However, keeping in mind that we injected miR126-5p into small parts of the whole gastrocnemius muscle and only once at P60, as well as the fact that the efficiency of the procedure of the injection can also affect the efficacy of this treatment, we cannot rule out the possibility that a broader test of long-term efficacy will result in a stronger and more positive outcome. An alternative future study should address this issue by crossing a conditional tissue specific KO of miR126-5p mice with $SOD1^{G93A}$.

Considering that ALS is a multifactorial disease, and that miRs are predicted to regulate a wide range of metabolic and signaling pathways, manipulating their subcellular levels in neurons, muscles, or glia, miRs should generally be explored as a potential therapeutic strategy or tool for treatment of ALS and possibly other neurodegenerative diseases.

References

Arbour D, Tremblay E, Martineau É, Julien J-P, Robitaille R (2015) Early and persistent abnormal decoding by glial cells at the neuromuscular junction in an ALS model. J Neurosci 35:688–706.

Ben-Zvi A, Manor O, Schachner M, Yaron A, Tessier-Lavigne M, Behar O (2008) The Semaphorin receptor PlexinA3 mediates neuronal apoptosis during dorsal root ganglia development. J Neurosci 28:12427–12432.

Ben-Zvi A, Yagil Z, Hagalili Y, Klein H, Lerman O, Behar O (2006) Semaphorin 3A and neurotrophins: a balance between apoptosis and survival signaling in embryonic DRG neurons. J Neurochem 96:585–597.

Birger A, Besser E, Reubinoff B, Behar O (2015) A new impedance based approach to test the activity of recombinant protein--Semaphorins as a test case. Eur J Cell Biol 94:453–457.

Birger A, Ottolenghi M, Perez L, Reubinoff B, Behar O (2018) ALS-related human cortical and motor neurons survival is differentially affected by Sema3A. Cell Death Dis 9:256.

Buratti E (2015) Functional Significance of TDP-43 Mutations in Disease. Adv Genet 91:1–53.

De Winter F, Vo T, Stam FJ, Wisman LAB, Bär PR, Niclou SP, van Muiswinkel FL, Verhaagen J (2006) The expression of the chemorepellent Semaphorin 3A is selectively induced in terminal Schwann cells of a subset of neuromuscular synapses that display limited anatomical plasticity and enhanced vulnerability in motor neuron disease. Mol Cell Neurosci 32:102–117.

Deumens R, Jaken RJP, Marcus MAE, Joosten EAJ (2007) The CatWalk gait analysis in assessment of both dynamic and static gait changes after adult rat sciatic nerve resection. J Neurosci Methods 164:120–130.

Di Pietro L, Baranzini M, Berardinelli MG, Lattanzi W, Monforte M, Tasca G, Conte A, Logroscino G, Michetti F, Ricci E, Sabatelli M, Bernardini C (2017) Potential therapeutic targets for ALS: MIR206, MIR208b and MIR499 are modulated during disease progression in the skeletal muscle of patients. Sci Rep 7:9538.

Dobrowolny G, Aucello M, Rizzuto E, Beccafico S, Mammucari C, Bonconpagni S, Belia S, Wannenes F, Nicoletti C, Del Prete Z, Rosenthal N, Molinaro M, Protasi F, Fanò G, Sandri M, Musarò A, Musarò A (2008) Skeletal Muscle Is a Primary Target of SOD1G93A-Mediated Toxicity. Cell Metab 8:425–436.

Dupuis L, Gonzalez de Aguilar J-L, Echaniz-Laguna A, Loeffler J-P (2006) Mitochondrial dysfunction in amyotrophic lateral sclerosis also affects skeletal muscle. Muscle Nerve 34:253–254.

Emde A, Hornstein E (2014) miRNAs at the interface of cellular stress and disease. EMBO J 33:1428–1437.

Fischer LR, Culver DG, Tennant P, Davis AA, Wang M, Castellano-Sanchez A, Khan J, Polak MA, Glass JD (2004) Amyotrophic lateral sclerosis is a distal axonopathy: evidence in mice and man. Exp Neurol 185:232–240.

Frey D, Schneider C, Xu L, Borg J, Spooren W, Caroni P (2000) Early and selective loss of neuromuscular synapse subtypes with low sprouting competence in motoneuron diseases. J Neurosci 20:2534–2542.

Fujita H, Zhang B, Sato K, Tanaka J, Sakanaka M (2001) Expressions of neuropilin-1, neuropilin-2 and semaphorin 3A mRNA in the rat brain after middle cerebral artery occlusion. Brain Res 914:1–14.

Gerber YN, Sabourin J-C, Rabano M, Vivanco M d M, Perrin FE (2012) Early Functional Deficit and Microglial Disturbances in a Mouse Model of Amyotrophic Lateral Sclerosis Cai H, ed. PLoS One 7:e36000.

Gurney ME, Pu H, Chiu AY, Dal Canto MC, Polchow CY, Alexander DD, Caliendo J, Hentati A, Kwon YW, Deng HX (1994) Motor neuron degeneration in mice that express a human Cu,Zn superoxide dismutase mutation. Science 264:1772–1775.

Haramati S, Chapnik E, Sztainberg Y, Eilam R, Zwang R, Gershoni N, McGlinn E, Heiser PW, Wills A-M, Wirguin I, Rubin LL, Misawa H, Tabin CJ, Brown R, Chen A, Hornstein E (2010) miRNA malfunction causes spinal motor neuron disease. Proc Natl Acad Sci U S A 107:13111–13116.

Hawley ZCE, Campos-Melo D, Droppelmann CA, Strong MJ (2017) MotomiRs: miRNAs in Motor Neuron Function and Disease. Front Mol Neurosci 10:127.

Ilieva H, Polymenidou M, Cleveland DW (2009) Non-cell autonomous toxicity in

neurodegenerative disorders: ALS and beyond. J Cell Biol 187:761–772.

Ionescu A, Zahavi EE, Gradus T, Ben-Yaakov K, Perlson E (2016) Compartmental microfluidic system for studying muscle–neuron communication and neuromuscular junction maintenance. Eur J Cell Biol 95:69–88.

Jaarsma D, Teuling E, Haasdijk ED, De Zeeuw CI, Hoogenraad CC (2008) Neuron-specific expression of mutant superoxide dismutase is sufficient to induce amyotrophic lateral sclerosis in transgenic mice. J Neurosci 28:2075–2088.

Jiang SX, Whitehead S, Aylsworth A, Slinn J, Zurakowski B, Chan K, Li J, Hou ST (2010) Neuropilin 1 Directly Interacts with Fer Kinase to Mediate Semaphorin 3A-induced Death of Cortical Neurons. J Biol Chem 285:9908–9918.

Kaneko S et al. (2006) A selective Sema3A inhibitor enhances regenerative responses and functional recovery of the injured spinal cord. Nat Med 12:1380–1389.

Kaplan A, Spiller KJ, Towne C, Kanning KC, Choe GT, Geber A, Akay T, Aebischer P, Henderson CE (2014) Neuronal matrix metalloproteinase-9 is a determinant of selective neurodegeneration. Neuron 81:333–348.

Kolodkin AL, Levengood D V, Rowe EG, Tai Y-T, Giger RJ, Ginty DD (1997) Neuropilin Is a Semaphorin III Receptor. Cell 90:753–762.

Körner S, Böselt S, Wichmann K, Thau-Habermann N, Zapf A, Knippenberg S, Dengler R, Petri S (2016) The Axon Guidance Protein Semaphorin 3A Is Increased in the Motor Cortex of Patients With Amyotrophic Lateral Sclerosis. J Neuropathol Exp Neurol:nlw003.

Lee J, Hyeon SJ, Im H, Ryu H, Kim Y, Ryu H (2016) Astrocytes and Microglia as Non-cell Autonomous Players in the Pathogenesis of ALS. Exp Neurobiol 25:233.

Lemmens R, Moore MJ, Al-Chalabi A, Brown RH, Robberecht W (2010) RNA metabolism and the pathogenesis of motor neuron diseases. Trends Neurosci 33:249–258.

Lino MM, Schneider C, Caroni P (2002) Accumulation of SOD1 mutants in postnatal motoneurons does not cause motoneuron pathology or motoneuron disease. J Neurosci 22:4825–4832.

Loeffler J-P, Picchiarelli G, Dupuis L, Gonzalez De Aguilar J-L (2016) The Role of Skeletal Muscle in Amyotrophic Lateral Sclerosis. Brain Pathol 26:227–236.

Luo Y, Raible D, Raper JA (1993) Collapsin: a protein in brain that induces the collapse and paralysis of neuronal growth cones. Cell 75:217–227.

Manzano R, Toivonen JM, Calvo AC, Oliván S, Zaragoza P, Muñoz MJ, Montarras D, Osta R (2012) Quantity and Activation of Myofiber-Associated Satellite Cells in a Mouse Model of Amyotrophic Lateral Sclerosis. Stem Cell Rev Reports 8:279–287.

Mead RJ, Bennett EJ, Kennerley AJ, Sharp P, Sunyach C, Kasher P, Berwick J, Pettmann B, Battaglia G, Azzouz M, Grierson A, Shaw PJ (2011) Optimised and Rapid Pre-clinical Screening in the SOD1G93A Transgenic Mouse Model of Amyotrophic Lateral Sclerosis (ALS) Deli MA, ed. PLoS One 6:e23244.

Miller TM, Kim SH, Yamanaka K, Hester M, Umapathi P, Arnson H, Rizo L, Mendell JR, Gage FH, Cleveland DW, Kaspar BK (2006) Gene transfer demonstrates

that muscle is not a primary target for non-cell-autonomous toxicity in familial amyotrophic lateral sclerosis. Proc Natl Acad Sci 103:19546–19551.

Molasy M, Walczak A, Szaflik J, Szaflik JP, Majsterek I (2017) MicroRNAs in glaucoma and neurodegenerative diseases. J Hum Genet 62:105–112.

Molofsky A V, Kelley KW, Tsai H-H, Redmond SA, Chang SM, Madireddy L, Chan JR, Baranzini SE, Ullian EM, Rowitch DH (2014) Astrocyte-encoded positional cues maintain sensorimotor circuit integrity. Nature 509:189–194.

Moloney EB, de Winter F, Verhaagen J (2014) ALS as a distal axonopathy: molecular mechanisms affecting neuromuscular junction stability in the presymptomatic stages of the disease. Front Neurosci 8:252.

Moloney EB, Hobo B, De Winter F, Verhaagen J, Schenone A, Azcoitia I (2017) Expression of a Mutant SEMA3A Protein with Diminished Signalling Capacity Does Not Alter ALS-Related Motor Decline, or Confer Changes in NMJ Plasticity after BotoxA-Induced Paralysis of Male Gastrocnemic Muscle Key B, ed. PLoS One 12:e0170314.

Mulder D, Kurland L, Offord K, Beard C (1986) Familial adult motor neuron disease: amyotrophic lateral sclerosis. Neurology 36:511–517.

Musarò A (2013) Understanding ALS: new therapeutic approaches. FEBS J 280:4315–4322.

Nachmany H, Wald S, Abekasis M, Bulvik S, Weil M (2012) Two potential biomarkers identified in mesenchymal stem cells and leukocytes of patients with sporadic amyotrophic lateral sclerosis. Dis Markers 32:211–220.

Nagai M, Re DB, Nagata T, Chalazonitis A, Jessell TM, Wichterle H, Przedborski S (2007) Astrocytes expressing ALS-linked mutated SOD1 release factors selectively toxic to motor neurons. Nat Neurosci 10:615–622.

Nakamura F, Kalb RG, Strittmatter SM (2000) Molecular basis of semaphorin-mediated axon guidance. J Neurobiol 44:219–229.

Perlson E, Jeong G-B, Ross JL, Dixit R, Wallace KE, Kalb RG, Holzbaur ELF (2009) A switch in retrograde signaling from survival to stress in rapid-onset neurodegeneration. J Neurosci 29:9903–9917.

Peters OM, Ghasemi M, Brown RH (2015) Emerging mechanisms of molecular pathology in ALS. J Clin Invest 125:1767–1779.

Philips T, Rothstein JD (2015) Rodent Models of Amyotrophic Lateral Sclerosis. Curr Protoc Pharmacol 69:5.67.1-21.

Rakhit R, Crow JP, Lepock JR, Kondejewski LH, Cashman NR, Chakrabartty A (2004) Monomeric Cu,Zn-superoxide dismutase is a common misfolding intermediate in the oxidation models of sporadic and familial amyotrophic lateral sclerosis. J Biol Chem 279:15499–15504.

Rosen DR et al. (1993) Mutations in Cu/Zn superoxide dismutase gene are associated with familial amyotrophic lateral sclerosis. Nature 362:59–62.

Rotem N, Magen I, Ionescu A, Gershoni-Emek N, Altman T, Costa CJ, Gradus T, Pasmanik-Chor M, Willis DE, Ben-Dov IZ, Hornstein E, Perlson E (2017) ALS Along the Axons – Expression of Coding and Noncoding RNA Differs in Axons of ALS models. Sci Rep 7:44500.

Scrutton N, Deonarain M, Berry A, Perham R, Cayabyab A, Hung W, Getzoff E, Hu

P, Herzfeldt B, Roos R, et al. (1992) Cooperativity induced by a single mutation at the subunit interface of a dimeric enzyme: glutathione reductase. Science (80-) 258:1140–1143.

Shi P, Wei Y, Zhang J, Gal J, Zhu H (2010) Mitochondrial Dysfunction is a Converging Point of Multiple Pathological Pathways in Amyotrophic Lateral Sclerosis Zhu X, Beal MF, Wang X, Perry G, Smith MA, eds. J Alzheimer's Dis 20:S311–S324.

Shirvan A, Kimron M, Holdengreber V, Ziv I, Ben-Shaul Y, Melamed S, Melamed E, Barzilai A, Solomon AS (2002) Anti-semaphorin 3A Antibodies Rescue Retinal Ganglion Cells from Cell Death following Optic Nerve Axotomy. J Biol Chem 277:49799–49807.

Tsitkanou S, Della Gatta PA, Russell AP (2016) Skeletal Muscle Satellite Cells, Mitochondria, and MicroRNAs: Their Involvement in the Pathogenesis of ALS. Front Physiol 7:403.

Van Battum EY, Brignani S, Pasterkamp RJ (2015) Axon guidance proteins in neurological disorders. Lancet Neurol 14:532–546.

Venkova K, Christov A, Kamaluddin Z, Kobalka P, Siddiqui S, Hensley K (2014) Semaphorin 3A signaling through neuropilin-1 is an early trigger for distal axonopathy in the SOD1G93A mouse model of amyotrophic lateral sclerosis. J Neuropathol Exp Neurol 73:702–713.

Villain G, Poissonnier L, Noueihed B, Bonfils G, Rivera JC, Chemtob S, Soncin F, Mattot V (2017) miR-126-5p promotes retinal endothelial cell survival through SetD5 regulatio in neurons. Development:dev.156232.

Vilmont V, Cadot B, Vezin E, Le Grand F, Gomes ER (2016) Dynein disruption perturbs post-synaptic components and contributes to impaired MuSK clustering at the NMJ: implication in ALS.

Wen X, Tan W, Westergard T, Krishnamurthy K, Markandaiah SS, Shi Y, Lin S, Shneider NA, Monaghan J, Pandey UB, Pasinelli P, Ichida JK, Trotti D (2014) Antisense proline-arginine RAN dipeptides linked to C9ORF72-ALS/FTD form toxic nuclear aggregates that initiate in vitro and in vivo neuronal death. Neuron 84:1213–1225.

Wen X, Westergard T, Pasinelli P, Trotti D (2016) Pathogenic determinants and mechanisms of ALS/FTD linked to hexanucleotide repeat expansions in the C9orf72 gene. Neurosci Lett.

Wong M, Martin LJ (2010) Skeletal muscle-restricted expression of human SOD1 causes motor neuron degeneration in transgenic mice. Hum Mol Genet 19:2284–2302.

Worzfeld T, Offermanns S (2014) Semaphorins and plexins as therapeutic targets. Nat Rev Drug Discov 13:603–621.

Zahavi EE, Ionescu A, Gluska S, Gradus T, Ben-Yaakov K, Perlson E (2015) A compartmentalized microfluidic neuromuscular co-culture system reveals spatial aspects of GDNF functions. J Cell Sci 128:1241–1252.

Zahavi EE, Maimon R, Perlson E (2017) Spatial-specific functions in retrograde neuronal signalling. Traffic.

Figure Legends

Figure 1 – Pre-symptomatic elevation in the levels of Sema3A and NRP1 in ALS models.

(A-B) Western-blot analysis of P30 and P60 GC muscle extracts revealed that the levels of Sema3A are elevated in pre-symptomatic SOD1^{G93A} muscles compared with their corresponding LM control wherein earlier stages, we found no significant difference (Figure 1-1). Tubulin was used as a loading control. P30: (Student's t-test, n=3, *p=0.042) P60: (Student's t-test, n=4, *p=0.038). (C) qPCR analysis of pre symptomatic P60 and P30 GC muscle extracts also shows an elevation in the mRNA levels of Sema3A in SOD1^{G93A} (Student's t-test, SOD1^{G93A} n=5, LM n=4, *p=0.049). (D) Immunostaining of primary myocytes after 7 days in culture shows elevated levels of Sema3A in primary myocytes of SOD1^{G93A}. White indicates Sema3A and blue indicates nuclear DAPI staining. Scale bars: 5μm. (E) Image analysis reveals an increase in Sema3A intensity in SOD1^{G93A} primary myocytes (Student's t-test, n=3, ~80 cells, ***p=0.00001). (F) Western blot analysis of primary myocyte-conditioned media revealed a higher level of Sema3A in the conditioned media of SOD1^{G93A}. Cultures were lysed after CM collection and equal loading volumes of lysates were immunoblotted for ERK to validate CM, which was produced from a similar mass of myocytes (Student's t-test, n=3, *p=0.018). (G-H) Immunostaining of fixed whole P60 GC muscles shows distinct Sema3A expression in the NMJs of SOD1^{G93A} mice. White indicates Sema3A, red indicates TMR-BTX labeling of Acetylcholine receptors on post synapse, and blue indicates presynaptic NFH in neurons. The percentage of muscle fibers expressing Sema3A in their NMJs in P60 SOD1^{G93A} mice is higher (~100 NMJ per 1 biological repeat; Student's t-test, SOD1^{G93A} n=4, WT n=3, *p=0.011). Scale bars: 10μm. We also examined Sema3A expression in later stages of the disease (Figure 1-2). (I) Western blot analysis of GC muscle extracts from P60 mice revealed elevated NRP1 levels in the muscles of SOD1^{G93A}. Tubulin was used as a loading control (Student's t-test, n=3, *p=0.048). (J) Western blot analysis of sciatic nerve (SN) extract from P60 mice shows an elevation in the levels of NRP1 in the sciatic nerves of SOD1^{G93A} mice (n=3). (K) Western blot analysis of primary MN lysates after 3 days in culture reveals an elevation in the NRP1 levels in SOD1^{G93A} MNs, that are not regulated by Sema3A binding (Figure 1-3). ERK was used as a loading control (Student's t-test, n=3, *p=0.031). (L-N) Immunostaining of primary MNs after 3 days in culture shows an elevation in the levels of NRP1 in both axons (inset, ~4.1-fold) and Somata (~1.9-fold) of SOD1^{G93A} motor neurons. White indicates NRP1; blue indicates NFH. Somata: (Student's t-test, n=3,~40 cells, ***p=0.00021);

axons: (Student's t-test, n=3,~40 cells, *p=0.012). Scale bars: 10μm. (O-P) Immunostaining of fixed whole P60 GC muscles shows distinct NRP1 expression in the NMJs of $SOD1^{G93A}$ mice. White indicates NRP1, red indicates BTX, and blue indicates NFH. The percentage of muscle fibers expressing NRP1 in their NMJs in P60 $SOD1^{G93A}$ mice is higher (Student's t-test, $SOD1^{G93A}$ n=4, WT n=3, *p=0.042). Scale bars: 5μm. We further examined NRP1 expression in later stages of the disease (Figure 1-2). Elevations in Sema3A and its co-receptor were found also in human sALS samples (Figure 1-4). Data in A-C, E-F, I-K, and M-N show the mean fold difference over the LM control ±SEM.

Figure 2 –Sema3A as well as primary myocytes expressing diverse ALS-causing mutations impair the growth of wild-type HB9::GFP motor axons and enhance their retraction and degeneration.

(A) Experimental procedure illustration and representative time-lapse images of HB9::GFP motor axons (Figure 2-1) in the distal compartment of a microfluidic chamber with no muscles after applying Sema3A to the distal compartment. After 6 hours, axons in the distal compartment of chambers that were treated with Sema3A undergo degeneration, whereas axons in the control chamber or axons co-treated with NRP1 antibody and Sema3A continue growing. Scale bar: 20μm. (B) Quantification of the rate of degraded axons in the distal compartment revealed a higher percentage of degradation in chambers that were exposed to Sema3A compared either to control or to co-application of Sema3A and NRP1 antibody (~60 axons for Sema3A treatment, ~70 axons for Control; Student's t-test; n=4; mean ±SEM, ***P=0.00022). (C) Schematic view of the experimental procedure in D-F. HB9::GFP spinal cord explants and primary myocytes of $SOD1^{G93A}$, $TDP43^{A315T}$, C9orf72-PR_{50}, C9orf72-GR_{50}, or LM, GFP, and $SOD1^{wt}$ as controls were co-cultured in a microfluidic chamber (Figure 2-2) and the growth of HB9::GFP axons was assessed by time-lapse imaging of the microgroove compartment. (D) Representative time-lapse images of the HB9::GFP axon growth when co-cultured with (left to right) LM, $SOD1^{G93A}$, and $SOD1^{G93A}$ +NRP1 antibody. The presence of $SOD1^{G93A}$ myocytes in the distal compartment triggers the retraction and degeneration of HB9::GFP motor axons growing in the groove compartment and prevents their traversing. When NRP1 antibody is applied to the distal compartment, together with $SOD1^{G93A}$-expressing myocytes, axons are less prone to degenerate. Scale bar, 5μm. (E) Quantification of the rate of axons traversing the distal compartment in B shows the mean percentage of axons that traversed the distal compartment out of the total axons in each field (n=3; NRP1 antibody experiment

n=4; Student's t-test, *p=0.025, *p=0.0433). (F) Quantification of the rate of axons traversing the distal compartment shows the mean percentage of axons that traversed the distal compartment out of the total number of axons in each field in co-culture with TDP43^{A315T}, C9orf72-PR$_{50}$, C9orf72-GR$_{50}$ myocytes, or GFP as a control. The traversing rate of HB9::GFP motor axons into the distal compartment in each of the co-cultures with muscle-expressing ALS mutations is significantly reduced (n=3; Student's t-test, GR$_{50}$*p=0.0137, PR$_{50}$*p=0.0374, TDP*p=0.0304. (G) Representative images of fixed and immunostained SOD1^{G93A} motor axons in the distal compartment of a microfluidic chamber after applying LM or SOD1^{G93A} myocyte CM to the distal compartment. After 48 hours, axons in the distal compartment of chambers that were treated with SOD1^{G93A} CM underwent degeneration, whereas axons that were treated with LM CM remained intact. WT MN axons remained intact after application of either conditioned media (Figure 2-3). When NRP1 antibody is applied to the distal compartment, together with SOD1^{G93A} CM, axons are less prone to degenerate suggesting the involvement of multiple factors (Figure 2-4). Green indicates Acetylated Tubulin. Scale bar, 20μm. (H) Quantification of the rate of degenerated SOD1^{G93A} axons in the distal compartment treated with control CM, SOD1^{G93A} CM, or SOD1^{G93A} CM that was co-incubated with anti-NRP1 antibody. (Student's t-test; n=3; ***p=5x10-7,*p=0.018).

Figure 3 – miR126-5p is depleted in SOD1^{G93A} muscles and regulates Sema3 and NRP expression.

(A) NanoString^{TM} chip screen heat map of significantly altered miRs in P60 muscles of SOD1^{G93A} compared to LM mice (extended table under Figure 3-1). Red and green indicate a high or low abundance of miRs, respectively; *p<0.05 (Student's t-test; n=3). (B) miR126-5p was the most significantly down-regulated miRNA in SOD1^{G93A} muscles (Student's t-test; n=3, **p=0.003). (C) qPCR analysis of P60 GC muscle extracts further validate the decrease in miR 126-5p in SOD1^{G93A} (n=3). (D-G) qPCR analysis of Sema3A, NRP1, Sema3B, and NRP2 transcript levels in HeLa cells overexpressing either miR126-5p or miR142 demonstrates a reduction in their expression levels specifically under miR126-5p overexpression (Student's t-test; n=3, *P=0.0438, *P=0.034, *P=0.031, *P=0.0434, respectively). (H) Representative TIRF images of U87MG cells reveal a detachment of the cell membrane from the culture dish surface after Sema3A is added to the culture medium. Scale bar, 10μm. (I) Impedance recording of live cells over time shows that U87MG cells overexpressing miR126-5p are unresponsive to Sema3A added to the culture medium, since their

impedance continuously increases, whereas the impedance of U87MG cells overexpressing miR142 decreases after treatment (Figure 3-2).

Figure 4 – Overexpression of miR126-5p in primary SOD1^{G93A} myocytes blocks motor axon degeneration and preserves neuromuscular junction activity in a compartmental co-culture.

(A-B) Western blot analysis of transfected myocyte extract overexpressing miR126-5p or miR142 and their conditioned media validates miR126-5p as a regulator of Sema3A specifically in muscles. ERK was used as a loading control (Student's t-test, n=3, *P=0.0499; *P=0.05, respectively). (C) Schematic view of the experimental procedure in (D-E). HB9::GFP spinal cord explants and primary myocytes of SOD1^{G93A} mice were co-cultured in a microfluidic chamber. The growth of the HB9::GFP axons was assessed both by time-lapse imaging of the microgroove compartment and by imaging axons that traversed the distal compartment. (D) Representative time-lapse images and quantification of HB9::GFP axon growth when co-cultured with SOD1^{miR126} myocytes (upper panel) or SOD1^{miR142} myocytes (lower panel). SOD1^{miR126} myocytes in the distal compartment enhanced the axonal traversal of the distal compartment as compared with the SOD1^{miR142} myocytes. The data are shown as the mean rate of axons that traversed the distal compartment out of the total number of axons in each field ±SEM (Student's t-test, n=3, *****p=0.04216). (E) Representative time-lapse images and quantification of HB9::GFP axon growth when co-cultured with PR_{50}^{miR126} myocytes (upper panel) or PR_{50}^{miR142} myocytes (lower panel). PR_{50}^{miR126} myocytes in the distal compartment enhanced the axonal traversal of the distal compartment compared with PR_{50}^{miR142} myocytes. The data are shown as the mean rate of axons that traversed the distal compartment out of the total number of axons in each field ±SEM (Student's t-test, n=3). (F) Representative myocyte contraction plot showing the bursting contractile behavior of innervated myocytes *in vitro*. (G) Quantification of the percentage of innervated myocytes that contract in a bursting pattern shows a diminished rate of bursting behavior in SOD1^{G93A} myocytes compared with LM controls. SOD1^{miR126} myocytes show an increase in the rate of bursting myocytes back to the LM levels. The data are shown as the mean percentage of bursting myocytes ± SEM (Student's t-test, n=3, *p=0.0291, *p=0.0156, **p=0.005656).

Figure 5 – pLL-eGFP-miR126-5p injected into GC muscles of pre-symptomatic SOD1^{G93A} mice transiently rescues the early phenotype appearance *in vivo.*

(A) Schematic view of the *in-vivo* experimental procedure. SOD1^{G93A} mice were injected with either pLL-eGFP-miR126-5p or pLL-eGFP-miR142 in their right or left GC muscles, respectively. Viral infection was validated (Figure 5-1) (B) Representative whole-mount NMJ immunostaining of ~P90 SOD1^{G93A} GC muscles injected with either miR126-5p or miR142 lenti vectors. Red indicates BTX and green indicates NFH + Synaptophysin in presynaptic neurons. Scale bar: 20 μm. (C) The percentage of innervated NMJs in miR126-5p-injected muscles is higher compared with its controls in both P90 and P120 (P90: Student's t-test, n=6, *p=0.0475, *p=0.001245 P120: Student's t-test, n=5, *p=0.043, *p=0.0096). (D) Representative histological images of P120 WT, SOD1^{G93A}, miR126-5p, and miR142 GC muscle cross sections after H&E staining. Scale bar: 100 um. (E) Semi-quantification of a GC cross section from D shows a significant increase in the minimal muscle fiber diameter of muscles that were injected with miR126-5p (P120: Student's t-test, n=4, *p=0.031). (F) Illustration of the CatWalk XT gait analysis system that monitors mouse footprints. (G) Gait analysis Mean Stand Index parameter indicates the speed at which the paw loses contact with the surface. The MSI for the P90 miR126-5p-injected limbs was significantly higher than for miR142-injected limbs (Student's t-test, *P=0.0355). (H) The Gait analysis percent single support parameter indicates the relative duration of contact of a single paw on the glass floor. The percentage in which the injected animals were used along the run with a single paw was significantly higher compared with SOD1^{G93A} mice and showed similarity to the WT control (Student's t-test, SOD1^{G93A}-Injected *p=0.0004, WT-SOD1^{G93A} *p=0.000003) (I) Gait analysis base of support parameter indicates the average width between the hind paws. The base of support of both P90- and P120-injected mice was significant higher compared with SOD1^{G93A} (Student's t-test, P90 SOD1^{G93A}-Injected *p=0.0000006, WT-SOD1^{G93A} *p=0.000007; P120 SOD1^{G93A}-Injected *p=0. 0.00003, WT-SOD1^{G93A} *p=0.000000009)

Figure 6 - **Alterations in Semaphorin3A regulation by miR126-5p trigger motor neuron degeneration in ALS.**

miR126-5p is a negative regulator of Sema3 signaling in skeletal muscles. Down-regulation of miR126-5p in ALS disease drives the overexpression and secretion of Sema3A and potentially other NMJ destabilizing factors in skeletal muscles. The down-regulation in miR126-5p in diseased MNs drives the overexpression of NRP1 specifically in axons. The excess binding and activation of the NRP1 receptor by its overexpressed ligand Sema3A as a result of miR126-5p alteration promotes NMJ disruption and axon degeneration in a spatially confined process.

Figure 1-1 – (Support Figure1). Sema3A protein levels in P7 SOD1^{G93A} GC muscle.

(A) Western blot analysis of P7 GC muscle extracts reveals that the levels of Sema3A (~95 kDa) are similar in pre-mature SOD1^{G93A} muscles compared with their corresponding LM control. ERK (-42-44 kDa) was used as a loading control. (The mean fold change over control: SOD^{G93A} 1.2 ± 0.74; LM 1 ± 0.42; Student's t-test, n=3, n=2, respectively; n.s)

Figure 1-2 – (Support Figure1). Sema3A and NRP1 expression in the NMJs of SOD^{G93A} mice at the age of P90 and P120

(A-B) The percentage of muscle fibers expressing Sema3A in their NMJs in P90 SOD1^{G93A} mice is higher than in LM (SOD^{G93A} 26.92% ± 5.07%; LM 8% ± 1.36% (~100 NMJ per 1 biological repeat; Student's t-test, SOD1^{G93A} n=3, WT n=3, *p=0.023982), whereas in P120 mice this difference was abolished (SOD^{G93A} 10.22% ± 2.61%; LM 9.89% ± 2.21% (~100 NMJ per 1 biological repeat; Student's t-test, SOD1^{G93A} n=3, WT n=3, n.s). (C-D) The percentage of muscle fibers expressing NRP1 in their NMJs in P90 SOD1^{G93A} mice is higher than in LM (SOD^{G93A} 29.17% ± 1.86%; LM 21.66% ± 2.09% (~100 NMJ per 1 biological repeat; Student's t-test, SOD1^{G93A} n=3, WT n=3, *p=0.02767), whereas in P120 mice this difference was abolished (SOD^{G93A} 14.26% ± 2.43%; LM 18.14% ± 1.67% (~100 NMJ per 1 biological repeat; Student's t-test, SOD1^{G93A} n=3, WT n=3, n.s)

Figure 1-3 – (Support Figure1). NRP1 levels in MN are not regulated by Sema3A binding.

(A) Western blot analysis of wild-type MN that were cultured in the presence or absence of Sema3A for 3 days indicate no alterations in the levels of NRP1 (120kDa) in the Sema3A-treated group. ERK (42-44 kDa) was used as a loading control (the mean fold difference in NRP1 levels over control treatment +Sema3A 0.78 ± 0.1; -Sema3A 1 ± 0.16; n=4, n.s).

Figure 1-4 – (Support Figure1). Sema3A and NRP1 elevations in human sALS patients and C9orf72-PR$_{50}$ mutant myocytes.

(A) Western blot analysis of hMSC lysate from sALS patients and healthy controls indicates Sema3A (~95 kDa) elevation in human patients. ERK (42-44kDa) was used as a loading control (the mean fold change over controls: sALS 1.3 ± 0.22; healthy controls 1 ± 0.2, n=4). (B) Western blot analysis of hMSC lysates from sALS patients and healthy controls indicates similar elevations of NRP1 (120kDa) in human

patients. ERK (42-44 kDa) was used as a loading control (the mean fold change over control: sALS 5.7 ± 1.5; healthy controls 1 ± 0.4; Student's t-test, n=4; *p=0.01). (C) Western blot analysis of primary myocyte culture extract reveals a higher level of Sema3A in C9orf72-PR_{50} mutant muscles compared with the m.Cherry control. (The mean fold change over controls: PR_{50} 2.89 ± 1; m.Cherry 1 ± 0.357, Student's t-test, n=3; *p=0.049.). (D) Western blot analysis of primary myocyte culture-conditioned media of the muscle used in C reveals a higher level of Sema3A in conditioned media of C9orf72-PR_{50} mutant muscles over control. (The mean fold change over controls: PR50 4.45 ± 1.37; m.Cherry 1 ± 0.3, Student's t-test, n=3; *p=0.029.)

Figure 2-1 – (Support Figure2). Micro-Fluidic-Chamber efficiently separates the distal axons from the proximal cell bodies and dendrites.

(A) Simplified illustration of the compartmentalized microfluidic chamber used to culture spinal cord explants and primary myocytes in two different compartments connected via parallel microgrooves. (B) Representative images of HB9::GFP motor axons co-cultured in the presence (left panel) or absence (right panel) of wild-type primary myocytes in a microfluidic chamber, showing that myocytes facilitate the directed traversal of HB9::GFP motor axons into the distal compartment. Scale bar, 100µm. (C) Quantitative analysis of the axonal traversal rate per chamber of HB9::GFP explant cultured in the presence or absence of myocytes, which shows a significant increase in the traversal of axons when myocytes are present in the distal compartment (the mean number of traversing axons per chamber after 3 days in culture: with myocytes 8.5±1.5; no myocytes 2.3±0.42 **P=0.0026; Student's t-test; n=6). (D) Immunostaining of a motor neuron culture in a MFC system for MAP2, TAU, and DAPI markers revealed that all neurites that traverse the distal side of the chambers are positive for TAU (axonal marker) and negative for MAP2 (dendritic marker). Red indicates MAP2, green indicates TAU, and blue indicates DAPI. Scale bar**:** 200 µm.

Figure 2-2 - (Support Figure2). Manipulated myocyte cultures showing no morphological differences compared to healthy ones

(A) Representative images of all of the following *in vitro* primary cultured myocytes (top to bottom) WT, $SOD1^{G93A}$, $TDP43^{A315T}$, C9orf72-PR_{50}, C9orf72-GR_{50}, miR126-5p, and miR142 at 12 DIV. Under all muscle culture conditions, similarity in morphology, fusion, and health was observed. Blue indicates DAPI. Scale bar: 50µm. (B) Quantitative analysis of the mean nuclei per myocyte for each of the described

conditions (the mean fold difference over the WT control ± sem: WT 1±0.09, $SOD1^{G93A}$ 1.1±0.08, $TDP43^{A315T}$ 0.94±0.07, C9orf72-GR_{50} 0.97±0.05, C9orf72-PR_{50} 1.16±0.06, miR126-5p 1.16±0.06, m5R142 1.5±0.07. (C) Immunostaining of LM and $SOD1^{G93A}$ primary myocytes revealed a similarity in differentiation under both conditions at 19 DIV. Nuclear DAPI staining shows peripherally distributed nuclei. Intensity measurements of both alpha-actinin and Ryanodine Receptor (RyR) revealed an opposing stripe-like structure indicating their maturation. Red indicates alpha-actinin, green indicates RyR , blue indicates DAPI. Scale bar**:** 200 µm.

Figure 2-3 - (Support Figure2). WT and SOD^{G93A} conditioned media applied on WT axons

(A) Representative images of fixed and immunostained WT motor axons in the distal compartment of a microfluidic chamber after applying LM or $SOD1^{G93A}$ myocytes (CM) to the distal compartment. After 48 hours, axons in the distal compartment of chambers that were treated with either $SOD1^{G93A}$ or WT CM remain intact. Green indicates Acetylated Tubulin. Scale bar, 20µm. (B) Quantification of the rate of degenerated WT axons in the distal compartment treated with WT CM or $SOD1^{G93A}$ CM (the mean percentage of degenerated axons per field: $SOD1^{G93A}$ 6.88% ± 1.7%; WT 7.47% ± 1.22%).

Figure 2-4 – (Support Figure2). Sema3B and NRP2 levels are elevated in the $SOD1^{G93A}$ ALS mouse model as well as in human sALS patients.

(A-B) Immunostaining of fixed whole P60 GC muscles shows distinct Sema3B expression in the NMJs of $SOD1^{G93A}$ mice. Green indicates Sema3B, red indicates postsynaptic Acetylcholine receptors labeled with BTX and blue indicates NFH in presynaptic neurons. The percentage of NMJs expressing Sema3B in P60 muscles is higher in $SOD1^{G93A}$ mice. **p<0.01 (Student's t-test, n=3) (the mean percentage of NMJs expressing Sema3B: $SOD1^{G93A}$ 49.3% ± 1%; LM 25% ± 2.5%). Scale bars: 5µm. (C-D) Immunostaining of fixed whole P60 GC muscles shows distinct NRP2 expression in the NMJs of $SOD1^{G93A}$ mice. Green indicates NRP2, red indicates postsynaptic Acetylcholine receptors labeled with BTX, and blue indicates NFH in presynaptic neurons. The percentage of NMJs expressing NRP2 in P60 muscles is higher in $SOD1^{G93A}$ mice. **p<0.01 (Student's t-test, n=3) (the mean percentage of NMJs expressing NRP2: $SOD1^{G93A}$ 50% ± 2%; LM 33.5% ± 4.5%). Scale bars: 5µm. Data show the mean fold difference over LM control ±SEM.

Figure 3-1 – (Support Figure3). NanoString miR chip screen reveals the most significantly altered miRs in the GC muscles of SOD1^{G93A} compared with LM mice.

List of the most significantly altered miRs detected in the muscles of P60 SOD1^{G93A} mice compared to their LM. Data were normalized to the 100 most abundant miRs in the tissue; *p<0.05 (Student's t-test; n=3). Only two miRs were significantly down-regulated in SOD1^{G93A} muscles: miR126-5p and miR133a; **p<0.01 (Student's t-test; n=3).

Figure 3-2 – (Support Figure3). U87MG impedance measurement after Sema3A application

(A) Western blot analysis of the U87MG cell line after 3 days in culture reveals the presence of NRP1 protein (~120kDa). The expression of NRP1 protein did not change after m.Cherry transfection. ERK (~42-44 kDa) was used as a loading control. (B) Impedance recording of live U87 cells over time shows the responsiveness to Sema3A within minutes after its application, unlike the cells that were treated with the control medium.

Figure 5-1 – (Support Figure5). Validation of pLL-eGFP-miR virus expression *in vitro & in vivo*

(A) Representative images of *in vitro* pLL-eGFP-miR-126-5p infection of both MNs culture (left panel) and muscle culture (right panel) demonstrate the pLL-eGFP-miR construct's ability to infect and be expressed specifically in those tissues. Titer: $6x10^9$ Scale Bar: 100um (B) Western blot analysis of GFP protein levels of pLL-eGFP-miR126-5p and pLL-eGFP-miR142-injected GC muscle extract compared to non-injected muscle tissues reveals an increase in the GFP protein level only in muscles that were injected with either pLL-eGFP-miR126-5p or pLL-eGFP-miR142 viruses. Transfected myocyte cultures overexpressing GFP were used as a positive control. (C) qPCR analysis of GFP mRNA levels in pLL-eGFP-miR126-5p and pLL-eGFP-miR142-injected GC muscle extract compared to non-injected muscle tissues reveals an increase in GFP transcripts only in muscles that were injected with either pLL-eGFP-miR126-5p or pLL-eGFP-miR142 viruses (the mean fold change over non-injection: +injection 6.98 ± 2.38; -injection 1; n=4; n=1, respectively). (D-E) Whole-muscle NMJ immunostaining of injected SOD1^{G93A} muscles with pLL-eGFP-miR126 or pLL-eGFP-miR142. Red indicates postsynaptic acetylcholine receptors labeled with BTX, gray indicates Sema3A. The percentage of NMJs expressing Sema3A in pLL-eGFP-miR126-injected muscles is lower compared with the pLL-eGFP-miR142-

injected muscle control (The mean percentage of NMJs expressing Sema3A: miR126-5p 16%± 1%; injection of miR142 26% ± 5%; Student's t-test, n=5, * p=0.03357).

Movie 1 - (Support Figure2). Sema3A control medium on HB9::GFP distal axons

Time-lapse image series of HB9::GFP axons in the distal compartment of a MFC with control medium added to the distal compartment. Scale bar, 50µm.

Movie 2 - (Support Figure2). Sema3A in the distal compartment drives the degeneration of HB9::GFP distal axons

Time-lapse image series of HB9::GFP axons in the distal compartment of a MFC with Sema3A added to the distal compartment. Scale bar, 50µm.

Movie 3 - (Support Figure2). HB9::GFP axonal growth toward SOD1^{G93A} myocytes

Time-lapse image series of HB9::GFP axons in the microgroove compartment of a MFC with SOD1^{G93A} myocytes in the distal compartment (top). Scale bar, 50µm.

Movie 4 - (Support Figure2). HB9::GFP axonal growth toward LM myocytes

Time-lapse image series of HB9::GFP axons in the microgroove compartment of a MFC with LM myocytes in the distal compartment (top). Scale bar, 50µm.

Movie 5 - (Support Figure4). Myocyte exhibiting bursting contracted behavior

Time-lapse image series of innervated SOD^{G93A} expressing miR126-5p myocyte exhibiting bursting contracted behavior. Scale bar, 25µm.

Movie 6 -(Support Figure4). Myocyte exhibiting non-bursting contracted behavior

Time-lapse image series of innervated SOD^{G93A} expressing miR142 myocyte exhibiting non-bursting behavior. Scale bar, 25µm.

Figure 1

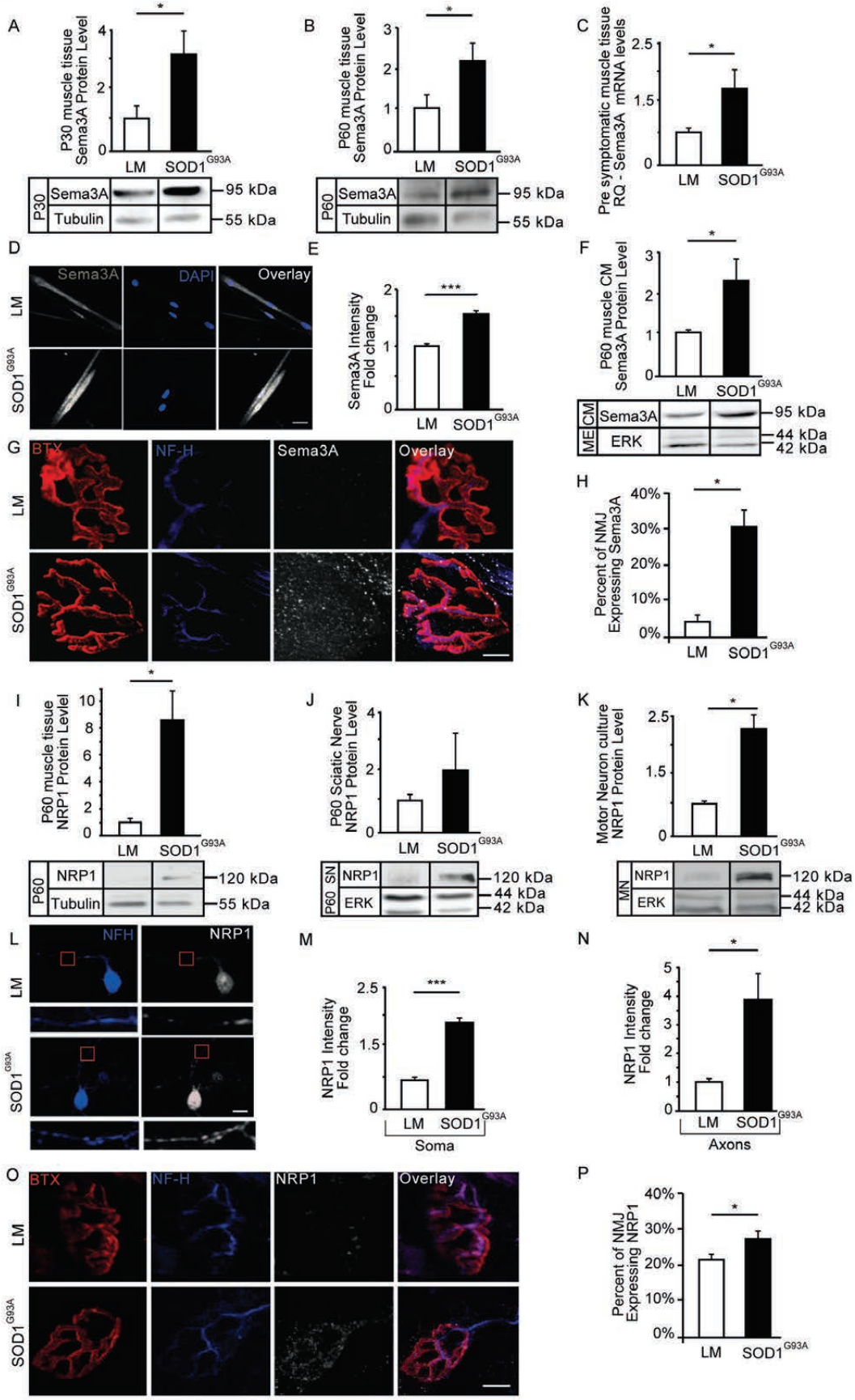

Figure 2

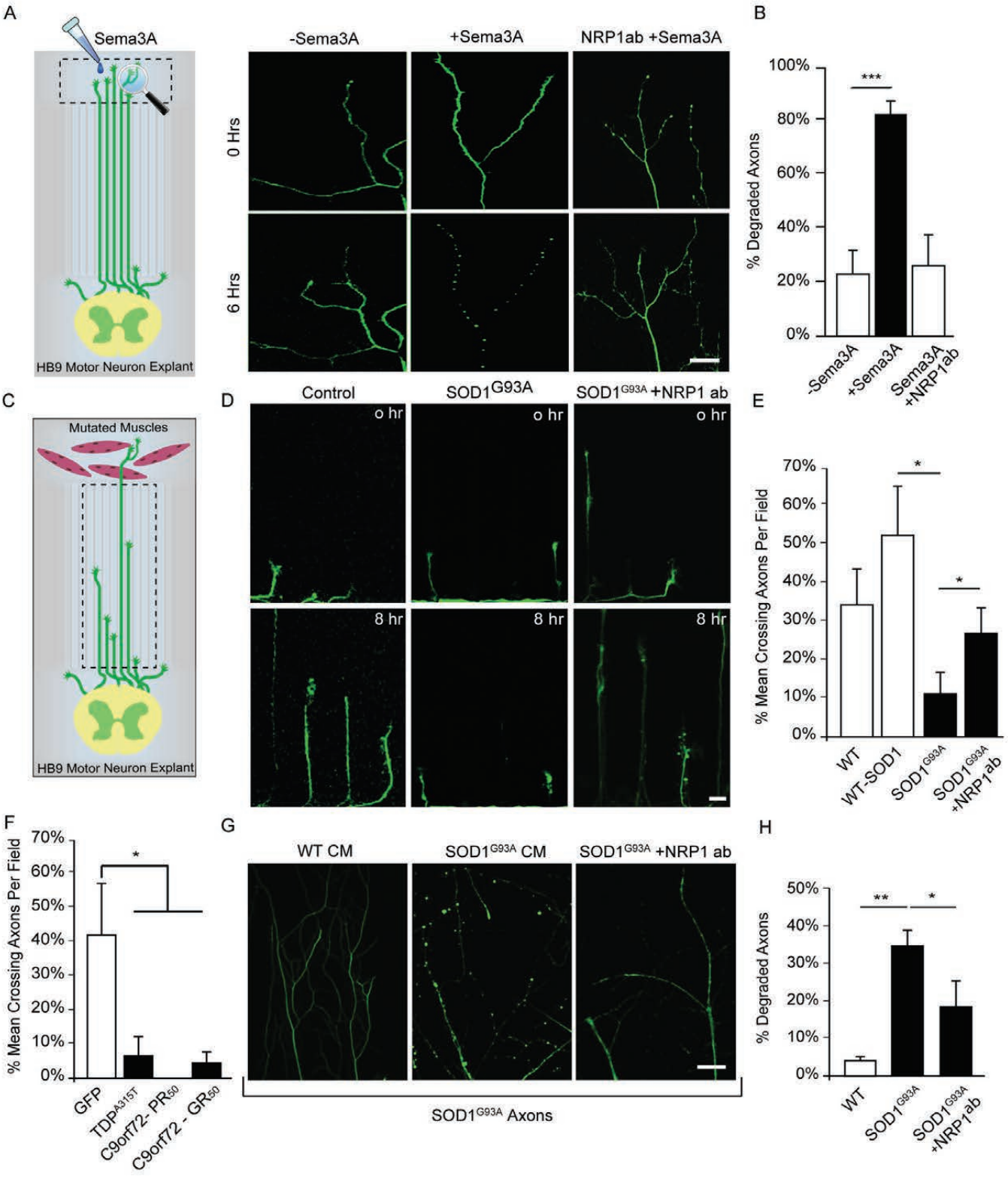

Figure 3

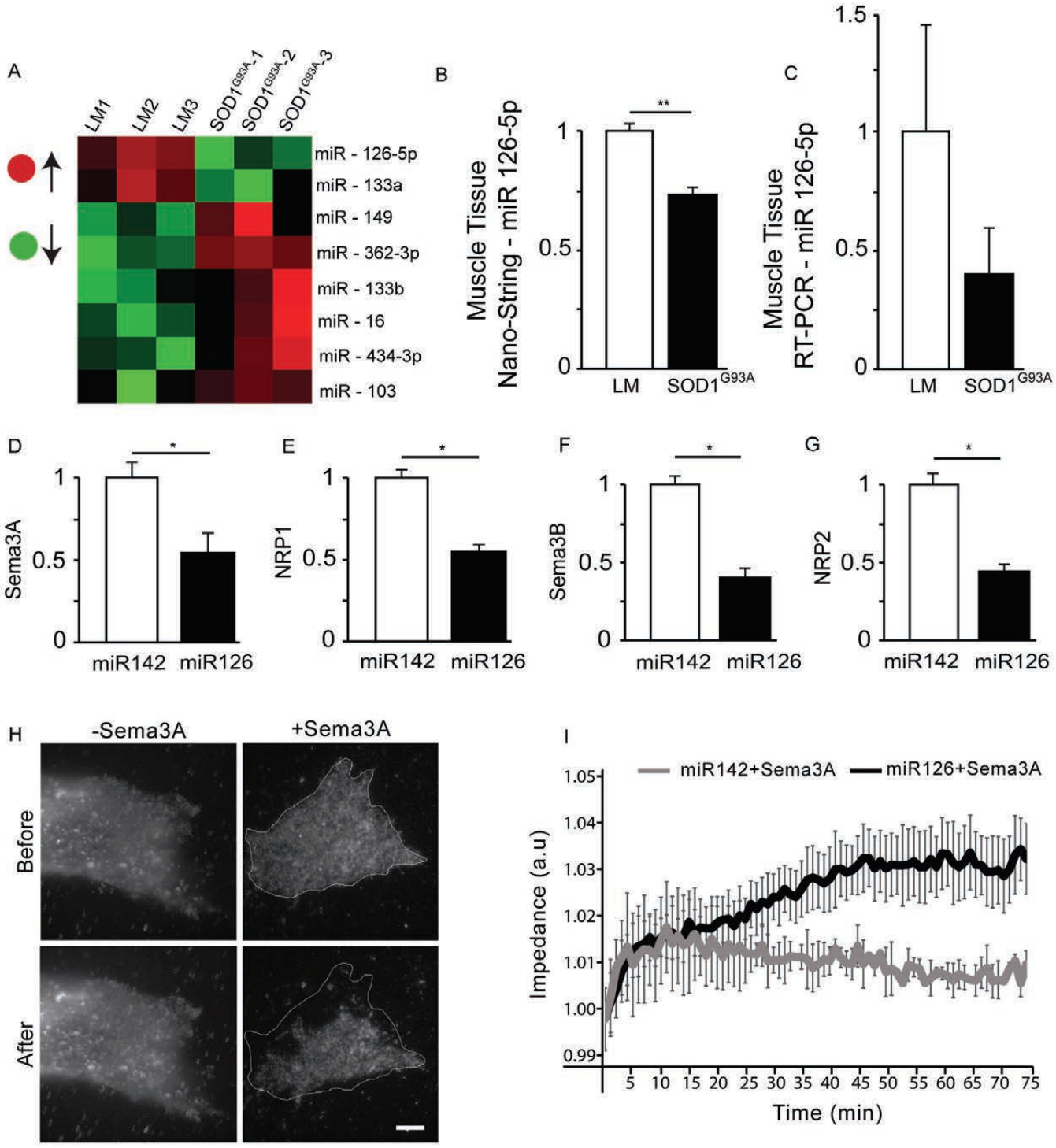

Figure 4

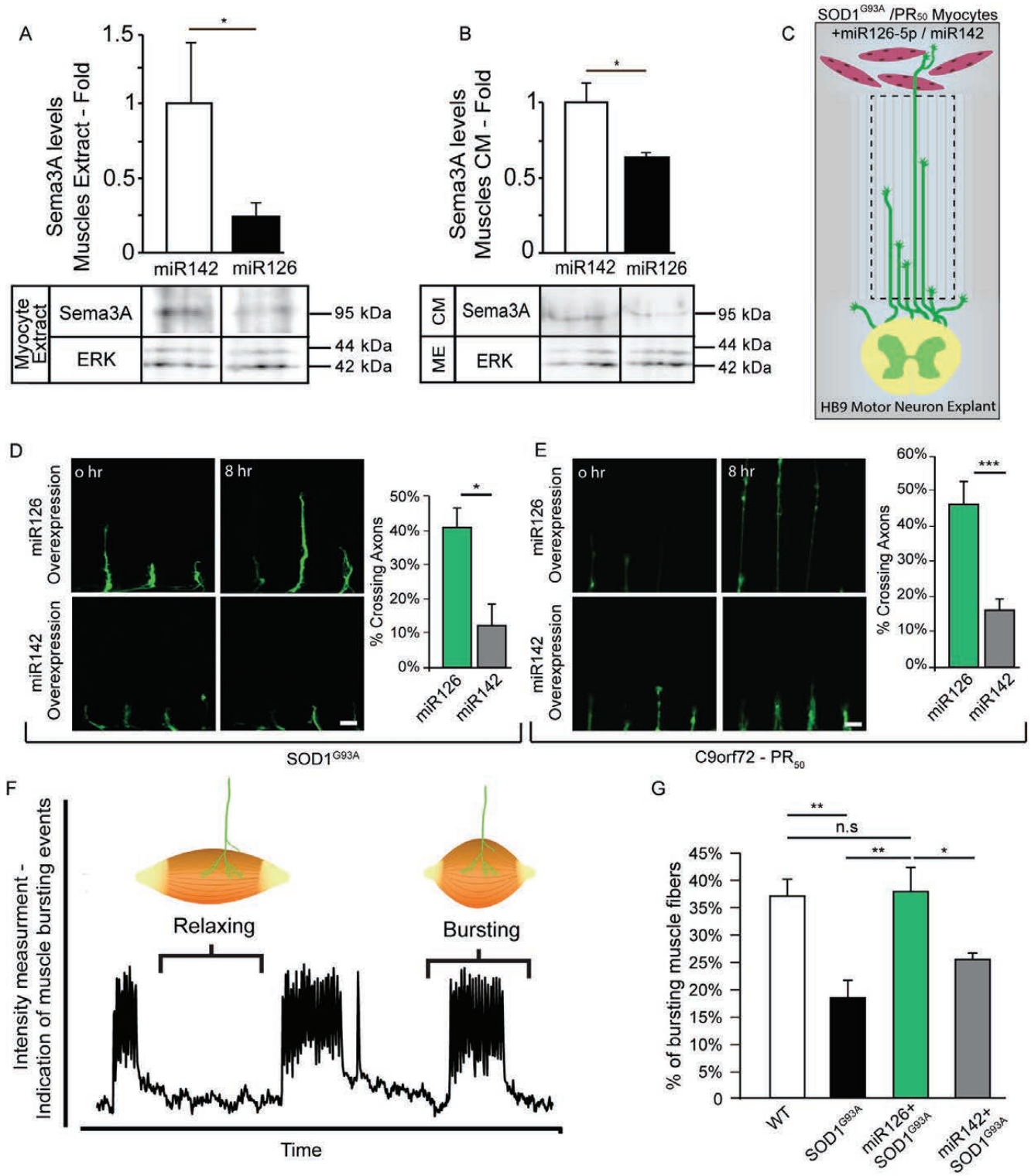

Figure 5

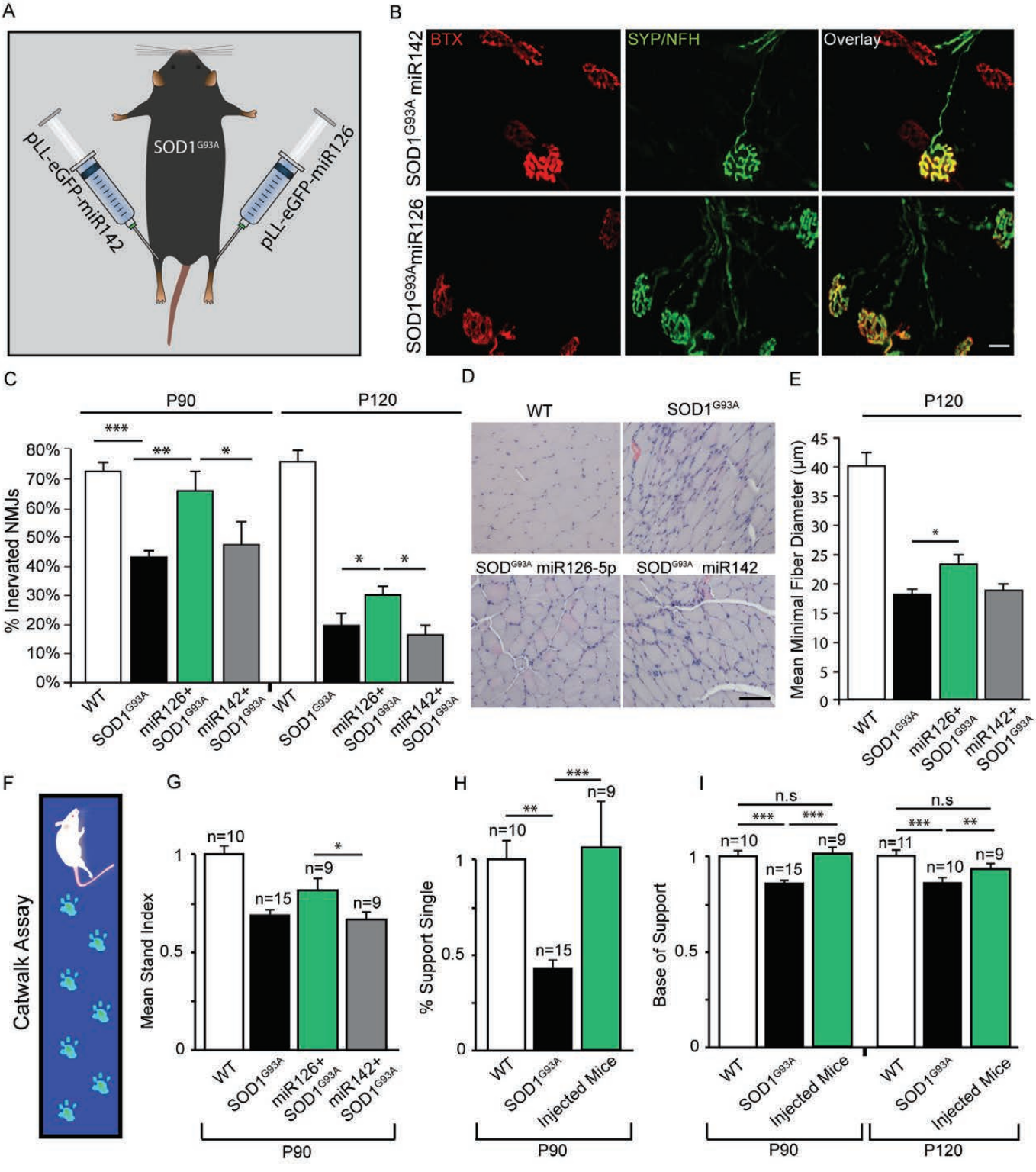

Figure 6

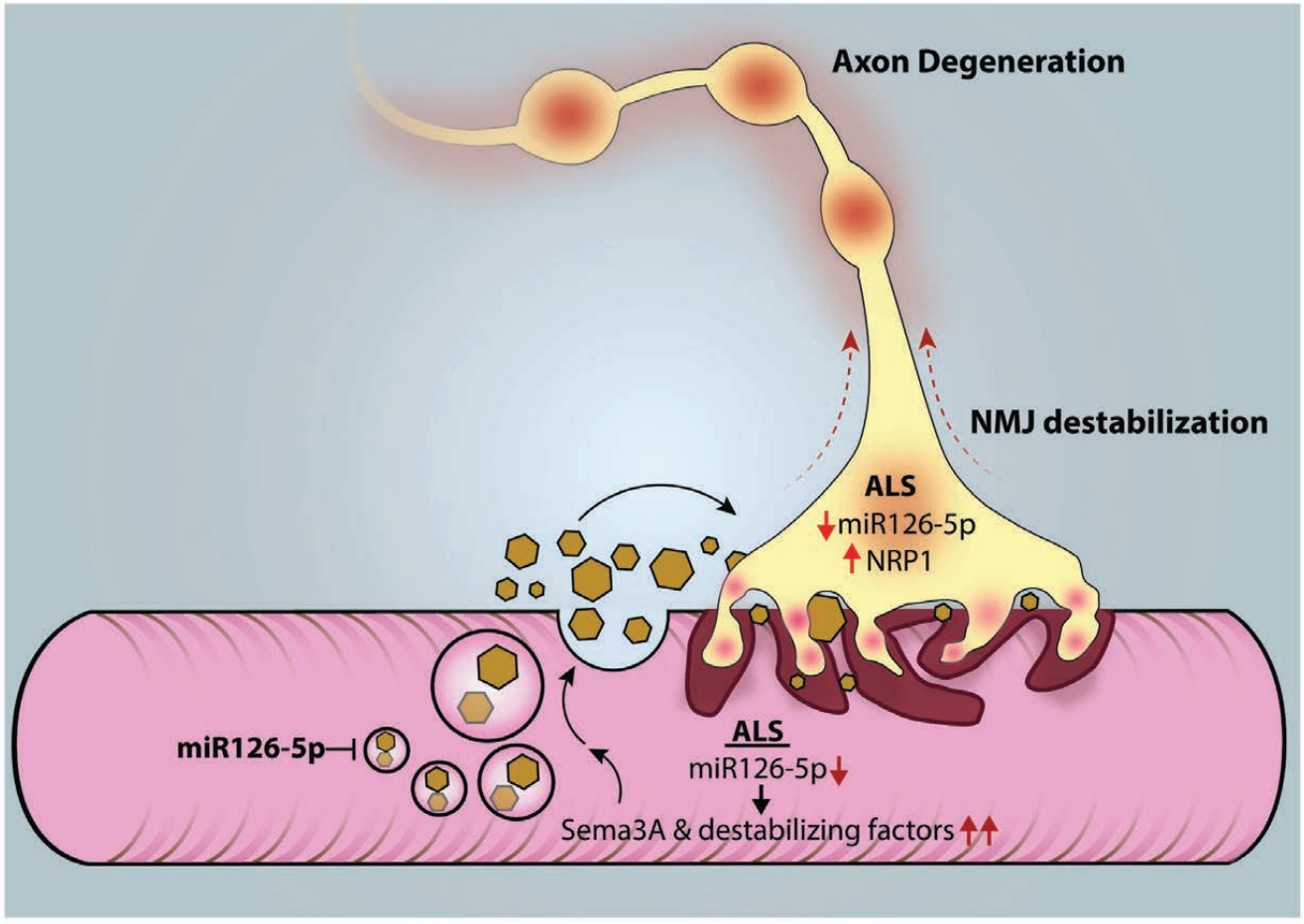

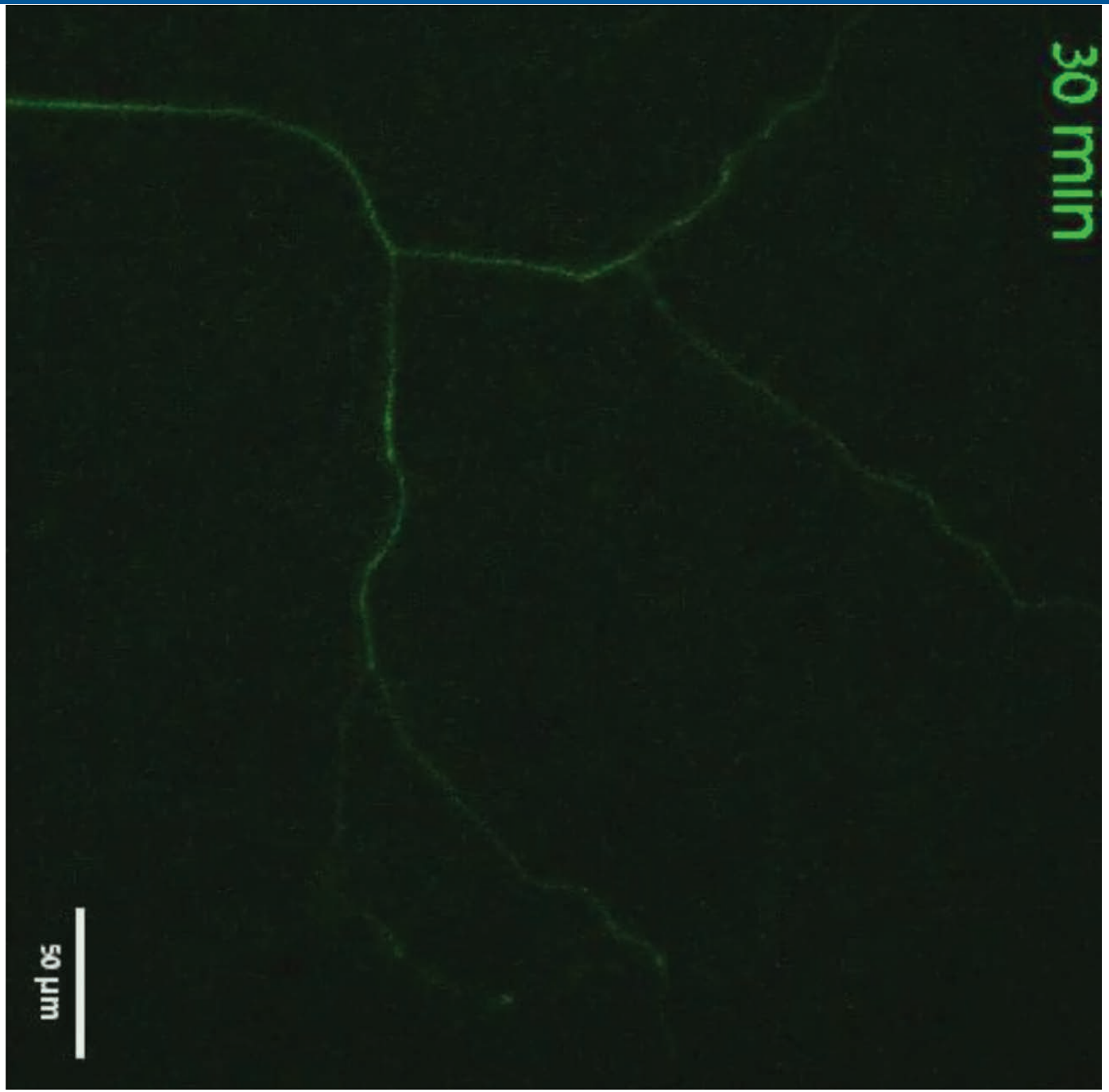
30 min
50 µm